

Automated Selection of Suitable Atmospheric Calibration Sites for Satellite Imagery

Robin Wilson

421985588

Summary:

A method was developed to automatically select suitable atmospheric calibration sites for satellite imagery, using a combination of various processing techniques followed by a fuzzy classification using eCognition. Desirable characteristics for calibration sites were identified from the literature, and implemented in a set of procedures combining ENVI/IDL processing routines and object-based classification using eCognition. Getis-Ord statistics were used to assess local patterns of spatial uniformity, and endmember abundances (extracted using the SMAACC algorithm) were used in a novel method to ensure a spread of calibration sites throughout the brightness range for each band.

The method was tested on a selection of medium- and high-resolution satellite imagery, and assessments of the quality of the selected calibration sites were provided by comparison with the identified desirable criteria, independent assessment by an expert and by performing an empirical line method calibration using the selected sites.

Results showed that the selected calibration sites were generally good calibration sites. The calibration produced an average accuracy of 38%, which compares poorly with results in the literature. However, this is unlikely to be a true reflection of the quality of the calibration sites, as many other factors combined to produce poor accuracies.

Table of Contents

1	Introduction	13
2	Aims and Objectives	15
3	Literature Review	17
3.1	Atmospheric Correction Techniques	17
3.2	Object-based Image Analysis	21
3.3	Spectral Endmembers.....	23
3.4	Local Indicators of Spatial Autocorrelation	24
4	Method.....	27
4.1	Study Images.....	27
4.2	Method Overview	28
4.3	Statistical calculation and thresholding.....	29
4.3.1	Assessing spatial uniformity: Getis statistics.....	29
4.3.2	Assessing spectral purity: Endmember extraction.....	31
4.3.3	Thresholding	31
4.3.4	Assessing flatness: Topographic Modelling.....	32
4.3.5	Automation and User Interface.....	32
4.4	Segmentation and classification	33
4.4.1	Segmentation	33
4.4.2	Fuzzy classification.....	36
4.4.3	Automation and export	41
4.5	Comparison with desirable criteria.....	41
4.5.1	Sites must be large	42
4.5.2	Sites must have a range of reflectances.....	42
4.5.3	Sites must be stable over time	42
4.5.4	Sites must be spatially homogenous	42
4.5.5	Sites must be flat	43
4.5.6	There must be two or more targets	43
4.5.7	Sites must be spread through the image	43
4.6	Independent assessment.....	43

4.7	Calibration Test	45
5	Results	47
5.1	Simulated IKONOS analysis	47
5.2	Calibration Site Locations	47
5.3	Comparison with desirable criteria.....	55
5.4	Independent Assessment	55
5.5	Calibration Test	56
6	Discussion.....	63
6.1	Comparison with desirable criteria.....	63
6.2	Independent Assessment	64
6.2.1	Temporal stability of sites	65
6.2.2	Spread of sites across the image	65
6.2.3	Adjacency effect problem.....	65
6.2.4	Exclusion of sawtooth roofs	66
6.2.5	Overall assessment.....	67
6.3	Quantitative Assessment	67
6.4	Possible Improvements.....	72
6.4.1	Quantitative Testing Improvements	72
6.4.2	Pixel Neighbourhood Influence Problem	73
7	Conclusions	75
8	Acknowledgements.....	77
9	References.....	79
10	Appendix A: Official Forms	87
11	Appendix B: Getis statistic problem	93
11.1	Problem Statement.....	93
11.2	Investigation	93
11.2.1	Test 1.....	93
11.2.2	Test 2.....	93
11.2.3	Further Tests	94
11.3	Impact.....	94
12	Appendix C: Shrunk calibration site analysis.....	95

13 Appendix D: IDL Source Code 97

Table of Figures

Figure 1 - Overview of process in setting up NCTAC. Red area shows contribution of this project.....	13
Figure 2 - Locations of the images used in this study	27
Figure 3 - Overview of the method showing input and output data	29
Figure 4 - Example Getis image (subset of Chilbolton image). Black pixels represent uniform areas (either dark or bright).	30
Figure 5 - Overview of the processing and thresholding steps carried out in ENVI/IDL	33
Figure 6 - Subset of the Chandlers Ford image showing segmentation at Level 2 (top) and Level 1 (bottom)	35
Figure 7 - eCognition class hierarchy. Values specified with X -> Y represent a continuous membership function from X to Y (see text). Classes inherit all rules from the classes above them.	38
Figure 8 - Example of a sawtooth roof on an industrial building in Eastleigh (within the Chandlers Ford IKONOS image). Photographer: Colin Smith, from www.geograph.org.uk	39
Figure 9 - Aerial photograph of a building in the Chalcroft Distribution Park (Chandlers Ford image). The sawtooth nature of the roof can clearly be seen. (Google Earth, 2009)	40
Figure 10 - Membership function graph used for the three fuzzy rules (<i>Like Endmember</i> , <i>Bright Uniform</i> and <i>Dark Uniform</i>). It can be seen that a membership value of 0.5 will be given to an image object which has 75% of its pixels selected as being like endmembers.	41
Figure 11 – Histogram of the pixels selected as calibration sites in band 3 of the Chilbolton image (red line) and histogram of all of the pixels in the image (black line) showing that the pixels selected as calibration sites are some of the brightest and darkest pixels in the scene.	44
Figure 12 - A subset of the Chilbolton image showing dark uniform areas in green and bright uniform areas in yellow, according to the Getis statistic thresholding.....	45
Figure 13 - Calibration sites selected within the Chandlers Ford image.....	49
Figure 14 - Calibration sites selected within the Kirkbride image.....	50
Figure 15 - Calibration sites selected within the Risley image	51
Figure 16 - Calibration sites selected within the Thorne Moor image (rotated 90° anticlockwise)	52

Figure 17 - Calibration sites selected within the Chilbolton image.....	53
Figure 18 - CASI image overlain on the SPOT image showing the relatively small area where data is available from both images	58
Figure 19 - Average spectra from the calibration sites selected for the calibration, showing the similarity of the three lake spectra.....	59
Figure 20 - Subset of SPOT image showing the calibration sites used in the calibration. Inset shows location of image in SPOT scene.	60
Figure 21 - Graph showing the percentage differences calculated between the corrected SPOT and CASI images, with the three SPOT bands marked.....	61
Figure 22 - Images of Chalcroft Distribution Park from the Chandlers Ford image (left) and Google Earth (right, from Google Earth, 2009) showing the selection only of non-sawtooth roofs.....	66
Figure 23 - Subset of Risley image showing oversegmentation of a building roof, with each sawtooth segment represented in a separate image object.....	67
Figure 24 - 3D graph of the pixel cloud from the SPOT data with points marked showing the calibration sites used. The red label is the building roof, the blue label is the average spectra from the lakes and the green label shows where a vegetation calibration site would be placed if one had been available.	69

Table of Tables

Table 1 - Summary of most common methods of atmospheric correction.....	19
Table 2 - Overview of the desirable criteria for atmospheric calibration sites.....	20
Table 3 - Parameters used for segmentation in eCognition	34
Table 4 - List of customised features implemented in eCognition, including explanations and calculations used to create them.....	36
Table 5 - Comparison of rules implemented in eCognition and the desirable characteristics of a calibration site.....	37
Table 6 - Qualitative assessment of calibration site selection by Dr Angela Harris.....	55
Table 7 - Comparison of the desirable criteria for calibration sites with the calibration sites selected in each image using the methods specified in section 4.5 (p41).	57
Table 8 - Information on the calibration targets used in the quantitative assessment.	58
Table 9 - Average percentage differences between the corrected SPOT and CASI images for a selection of pixels of different surface types	59
Table 10 - Percentage differences between the corrected SPOT and CASI images for each individual pixel of each surface type	61
Table 11 - Problems with the calibration performed in this study, and their causes....	70
Table 12 - Reported accuracies and other details for a number of applications of atmospheric correction approaches in the literature	71
Table 13 - Pixel values for both areas used in Test 1 of the Getis statistic problem	93
Table 14 - Pixel values for both areas used in Test 2 of the Getis statistic problem	94
Table 15 - Extract from the central section of the SPOT PSF derived by Ruiz and Lopez (Ruiz & Lopez, 2002). The shaded cell represents the pixel the sensor is observing.....	95
Table 16 - Differences between the percentage error for the normal calibration and the calibration with shrunk calibration sites. Differences are absolute differences in percentage points.....	96

1 Introduction

Atmospheric correction is an essential part of most remote sensing projects, but it can be time-consuming and requires a skilled analyst for best results. The selection of calibration sites for empirical methods of atmospheric correction is a vital part of the process, and the quality of the selected sites has a major influence on the overall accuracy of the calibration. This project will investigate the possibility of automating the selection of these calibration sites by a method utilizing statistical information from the image, thus allowing site selection to be performed in an objective and repeatable manner.

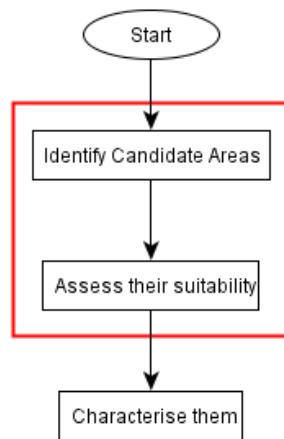


Figure 1 - Overview of process in setting up NCTAC. Red area shows contribution of this project.

If this project is successful, then the resulting procedure will be of great use to the remote sensing community. Analysts will be able to focus on the requirements of their projects, rather than spending considerable time attempting to select sites to perform an accurate calibration. The procedure developed by this project could prove useful in other areas such as:

- Selection of best locations for instrumented calibration sites (such as those suggested by the GIANTS project (Teillet et al., 2001) and the proposed Network of Calibrated Targets for Atmospheric Correction (NCTAC; Research proposal to NERC, E. J. Milton, personal communication, 2009)) from image data covering wide areas. Figure 1 shows the overall process in setting up NCTAC, as defined by Prof E. J.

Milton (personal communication, 2009) with the steps in which this project will play a part highlighted in red.

- Selection of the most appropriate parts of large vicarious calibration sites such as those listed on the USGS's Calibration-Validation site listing (USGS, 2009) including such sites as Tuz Golu, Turkey and White Sands, New Mexico.
- Selection of pseudo-invariant features for use in image-to-image normalisation (for example Davranche et al., 2009).

This project should help atmospheric correction to become 'operational' (as defined by Teillet et al., 1997).

2 Aims and Objectives

The aim of this project is:

To develop an automated system to identify suitable targets for atmospheric correction of medium and high resolution satellite imagery.

Three objectives have been formulated, although it should be noted that successful completion of these objectives does not necessarily mean successful fulfilment of the aim:

1. To develop a set of criteria which can be used to select calibration sites for atmospheric correction.
2. To implement a automatic site selection routine based on these criteria using ENVI/IDL and eCognition.
3. To assess the quality of the calibration site selection both qualitatively and quantitatively

3 Literature Review

3.1 Atmospheric Correction Techniques

Remote sensing data are recorded as Digital Numbers (DNs), but these should not be used for further analysis as they are vulnerable to changes in atmospheric properties and illumination angles. Instead most analysis is performed with data which have been calibrated to surface reflectance factor (the ratio of directional reflected radiation to the incident radiation). Atmospheric correction, as well as correcting for the absolute calibration of the sensor, is required to convert DN's to the surface reflectance factor. This correction is essential before the data is used quantitatively (as suggested by Swain & Davis, 1978).

Table 1 provides an overview of atmospheric correction methods with their advantages and disadvantages. It can be seen that the Empirical Line Method and Revised Empirical Line Method provide a good 'middle ground' between the Dark Object Subtraction and Radiative Transfer Model methods, and the selection of calibration sites for these methods will be the focus of this study. The Empirical Line Method has been used as a pre-processing step in many projects (for example, de Jong, 1998; Malthus & Karpouzli, 2003), and commercial organisations such as Ordnance Survey are investigating using it routinely (E. J. Milton, personal communication, 2009). In fact, there is evidence that correction with the Empirical Line Method can enhance certain features which make it easier for spectral feature extraction methods to work (Dwyer et al., 1995).

High quality selection and characterisation of calibration sites is essential to providing high quality ELM corrections (Smith & Milton, 1999). An overview of the desirable criteria for a calibration site, according to the literature, is given in Table 2. Impervious surfaces (such as asphalt car parks (Smith & Milton, 1999) and bright flat building roofs) are often used for calibration sites, but these can be difficult to find in rural areas. However, in the UK there are a large number of abandoned military airfields (over 1,500 in total; Woodside, 2009) spread across much of the country. Impervious surfaces (such as runways and taxiways) often still exist on these airfields, and these

can provide good target sites. However, it should be noted that many airfields are now subject to other uses (Gallent et al., 2000), and that the temporal stability of unmaintained concrete is not assured. The temporal stability of bright building roofs may be better. For example Bretz and Akbari (1997) found that, for the majority of high-albedo roof coverings, the drop in albedo occurred mostly during the first year, and that the albedo was relatively stable after that.

In the absence of impervious surfaces, Moran et. al. (2001) suggested that the best rural targets are packed earth roads or car parks and rough bare soil surfaces. Large expanses of water are often used as dark targets, particularly in NIR bands, but it should be ensured that the water is deep enough to reduce the amount of surface glint which contributes to the overall reflectance.

For the Empirical Line Method to work effectively, various assumptions have to hold. These are outside of the scope of this project, but deserve mentioning:

- That there is a linear relationship between sensor Digital Number and the reflectance of ground targets. This has recently been shown to be true for a selection of Landsat TM pixels (Baugh & Groeneveld, 2008).
- That the same area is measured on the ground and from the satellite sensor. This can be particularly difficult, especially when upscaling from the scale of individual field spectroscopy measurements to satellite pixel sizes (Hamm et al., 2003). This is one of the main reasons that uniformity is desired, as this ensures that positional inaccuracies in the ground measurements do not cause a problem.
- That the ground measurement is taken at the same time as the sensor overpass. This is often difficult to achieve, which is why ground calibration targets which are stable over time are desired, as this can allow the ground measurements to be taken at a different time from the sensor overpass.

The empirical line method has also been shown to work effectively with a range of medium to high resolution satellite imagery such as Landsat (Moran et al., 2001) and IKONOS (Karpouzli & Malthus, 2003), as well as airborne imagery (such as CASI; Smith & Milton, 1999).

Table 1 - Summary of most common methods of atmospheric correction

Method	Explanation	Advantages	Disadvantages	References
Dark Object Subtraction (DOS)	Dark pixels are located, where the DN could reasonably be expected to be zero (for example water in the NIR wavelengths). The non-zero values found in these pixels are subtracted from every other pixel in the image as these values are assumed to represent the contribution of atmospheric scattering.	<ul style="list-style-type: none"> • Very simple • Requires no extra data 	<ul style="list-style-type: none"> • Often provides poor results • Assumes the effect of the atmosphere is constant across the image • Assumes that the only effect of the atmosphere is to increase DNs through atmospheric scattering 	Chavez (1996) Examples of use: Wu et al. (2005) for correcting images of cropland. Cohen et al. (2003) in a comparison of Landsat and MODIS.
Empirical Line Method (ELM)	Ground and satellite measurements of the same within-scene targets are used to produce a linear regression between Digital Number and reflectance factor.	<ul style="list-style-type: none"> • Can provide very high quality calibration, assuming the technique is carried out well • Requires no atmospheric data 	<ul style="list-style-type: none"> • Requires ground data, preferably contemporaneous with image acquisition • Assumes a linear relationship between sensor DN and ground reflectance factor 	Smith and Milton (1999) Examples of use: de Jong (1998) in a project examining tree damage by volcanic activity.
Refined Empirical Line Method (REL)	One within-scene bright target is selected and a simple radiative transfer model is used to provide the dark pixel DN. A linear regression is then performed, as above.	<ul style="list-style-type: none"> • Only requires one bright target, making calibration site selection easier • Combines the best of RTM and ELM 	<ul style="list-style-type: none"> • Requires ground data, preferably contemporaneous with image acquisition • Assumes a linear relationship between sensor DN and ground reflectance factor 	Moran et al. (2001) Examples of use: Xu and Huang (2006) to assess the accuracy of the method. Kutser et al. (2005) in a project to map organic matter in lakes.
Radiative Transfer Model (RTM)	A mathematical model is produced to model known physical processes occurring in the atmosphere, such as scattering. This is used to estimate the ground-level reflectance of each pixel.	<ul style="list-style-type: none"> • Based on the physics of light passing through the atmosphere • Produces the most accurate calibration (when performed with high quality atmospheric data) 	<ul style="list-style-type: none"> • Requires computationally intensive models to be run • Requires contemporaneous atmospheric data to ensure good calibration 	6S (Verote et al., 1997) MODTRAN (Berk et al., 1999) Examples of use: Matthew et al. (2000) to assess the accuracy of the method.

Table 2 - Overview of the desirable criteria for atmospheric calibration sites

Criterion	Justification
Large	The target must cover multiple pixels. The atmospheric adjacency effect is important here, as a dark target surrounded by bright surfaces would need to be larger to ensure that there are uncontaminated pixels in the centre of the target (due to the point spread function; Moran et al., 2001). It has been shown that a sensor resolution to target size ratio of 1:8 is needed to ensure that at least four pixels remain uncontaminated in the centre of the image (Slater, 1980).
Range of reflectances (preferably including very bright and very dark targets)	Selecting very bright and very dark targets ensures that both ends of the regression line are accurately placed (Smith & Milton, 1999). Ensuring a spread of targets across the range of brightnesses increases the accuracy of the regression line.
Stable over time	This is important as it means that the ground target does not need to be measured every time it is used in a calibration, as one can assume its reflectance is the same as last time it was measured (Moran et al., 2001). In practice this often means selecting areas that are devoid of vegetation (Moran et al., 2001). It should be noted that surface such as concrete, which are often assumed to be temporally stable, can in fact have significant changes over time (Anderson & Milton, 2006).
Spatially homogenous	Ensuring that a target is spatially homogenous reduces the importance of positional accuracy in the ground measurements and reduces the probability of mixed pixels occurring. Milton et al. (1997) showed that even very small scene elements can have a significant effect on spatially averaged reflectance. For example, they found an increase of up to 12% in the reflectance of a parking lot due to the presence of painted lines on the surface.
Flat	The reflectance of sloping targets changes dramatically with insolation angle, meaning that the time of data acquisition becomes very important. Also, it has been shown that the micro-topography of a surface is a major controller of its variability in reflection (Giardino & Brivio, 2003).

Criterion	Justification
Two or more targets	Early applications of the Empirical Line Method used two targets but recently it has been found that higher accuracies can be gained by using larger numbers of targets. Smith and Milton (1999) suggested that two targets are not enough, and Karpouzli and Malthus (2003) found that using nine targets gave a very high accuracy.
Sites spread throughout the image	A spread of sites throughout the image allows the variation in atmospheric conditions across the image to be accounted for.

3.2 Object-based Image Analysis

The problem of selecting suitable calibration sites can be approached as a classification problem, with the aim being to implement a suitable classification to differentiate between suitable and unsuitable calibration sites. Traditional methods of classifying remotely sensed images work on a per-pixel basis, assigning each individual pixel to one class. Object-based image analysis is a relatively new classification technique which involves segmenting the image into image objects (each consisting of a relatively homogenous area containing multiple neighbouring pixels) and then classifying these image objects, rather than the underlying pixels themselves (Blaschke et al., 2000). This allows properties of the image objects (such as the standard deviation of the pixel values, the area of the object or a measure of the texture of the object) to be used in the classification.

Object-based analysis is often used with high resolution sensors such as IKONOS. For example, Zhou & Troy (2008) used an object-oriented approach to classify the area surrounding Baltimore City, Maryland, USA and achieved an overall accuracy of 92.3%. Similarly, Zhou et al. (2009) found that classification of shadowed areas in high resolution urban imagery was more accurate when using an object-based classification method rather than a pixel-based method. Various other studies have shown that object-based classification approaches consistently provide higher accuracies than per-pixel approaches (Cleve et al., 2008; Thomas et al., 2003; Yan et al., 2006), especially when used with high-resolution data (Gao & Mas, 2008).

The quality of an object-oriented classification is dependent on the quality of the image segmentation, which should aim to produce relatively homogenous image objects. Meinel & Neubert (2004) emphasised this point, and provided a survey of image segmentation programs designed for use with remotely sensed data. They concluded that eCognition and InfoPACK (both commercial packages) provided the best segmentation, and that many other segmentation programs produced unacceptable results. eCognition's segmentation routine is based on a region-growing approach, and is described in detail in Benz et al. (2004) and Definiens Imaging (2004a).

Lu and Weng (2007) note that object-based classification approaches allow the use of spatial information (such as the topology of image objects) and textures as well as allowing easy use of both raster and vector data. They recommend both object-based image analysis and fuzzy classification (see below) as approaches to improve classification accuracy.

In a standard classification, each unit (pixel or image object) is assigned to one class. Fuzzy classifiers extend this to allow each pixel to belong to multiple classes, with a percentage membership specified for each class. For example, a pixel could have a 30% membership of the grass class, but a 70% membership of the trees class. Once a fuzzy classification has been performed the classification can be 'defuzzed', resulting in a standard classification with one class per image unit. Fuzzy classification provides an advantage to this project, as it allows the extent to which each image object fulfils the criteria for a calibration site to be quantified in the class membership function.

eCognition 4.0 is a commercial image processing package which combines both object-based classification and fuzzy classification. Complex class hierarchies can be defined using inheritance, allowing simple capture of class criteria, and each criterion can have a fuzzy membership function, allowing a fuzzy classification map to be produced. This is closer to the way that the human brain is thought to interpret images. Other object-based image classification software exists (such as the ENVI Feature Extraction module), but they are generally less powerful and less configurable than eCognition.

3.3 Spectral Endmembers

Earlier it was stated that it is desirable for the selected atmospheric calibration sites to have a range of reflectances, including very bright and very dark targets, and the use of spectral endmembers provides a suitable method of achieving this.

The spectral endmembers of an image are the purest pixels in the image, and they define the mixing space from which all other pixels are produced (Adams et al., 1993). Thus, the spectral endmembers are the most extreme pixels in the image, and define the edges of the pixel cloud. Therefore, if calibration sites are chosen which are close to the spectral endmembers of the image, they are certain to be some of the brightest and darkest pixels in each band.

This technique for selecting bright and dark pixels does not appear to be used in the literature although some authors have combined the selection of endmembers with object-based image analysis (for example Greiwe & Ehlers, 2005).

Various algorithms exist which extract the spectral endmembers from an image, and Martínez et al. (2006) provide an overview of some of the most popular. Many of these algorithms involve two stages: the extraction of the endmembers, and then the 'spectral unmixing' of the image to produce abundance images for each endmember where each pixel contains the percentage of each endmember spectrum which contributes to the spectra for that pixel.

The Pixel Purity Index (PPI; Boardman et al., 1995) projects the image data onto random unit vectors, counting the number of times each pixel appears as an extreme pixel in one of these projections. Using convex geometry, this count can be shown to be related to the purity of each pixel (Boardman, 1993). It should be noted that this procedure does not produce a list of endmembers as an output, but just an index of pixel purity which can guide an analyst as to which pixels may be endmembers (see, for example, the process followed in Rashed et al., 2003). The procedure is usually performed on images that have been transformed using the Minimum Noise Fraction (MNF; Green et al., 1988).

The Sequential Maximum Angle Convex Cone (SMACC; Gruninger et al., 2004) method identifies extreme vectors using a convex factorisation technique. The definition of an extreme vector is one which cannot be modelled by a positive linear combination of the existing extreme vectors, that is, the same as the definition of an endmember. Thus, the algorithm starts with a single endmember and creates new endmembers fulfilling the above criteria until it reaches a set limit. In contrast to PPI, this runs completely without intervention and performs automatic spectral unmixing, producing an output of abundance images for each endmember. It is also very fast when compared to PPI. As one of the more recent endmember extraction algorithms, the examples of use in the literature are sparse, but Lu and Weng (2006) used it in their analysis of the relationship between thermal features and landcover types in urban areas, and Knight et al. (2006) used it for producing landcover products from MODIS data.

3.4 Local Indicators of Spatial Autocorrelation

Spatial autocorrelation refers to the situation when the value of a variable at a certain location is related to values of the same variable at nearby locations, and local measures of spatial autocorrelation allow differences in autocorrelation across space to be observed. Many measures of spatial autocorrelation were originally designed to work with point data in GIS systems, but they can be applied to remotely sensed data with the locational information being provided by the pixels and the attribute data by the DN's. Various measures of spatial autocorrelation have been used with remote sensing data (see overview in Wulder & Boots, 1998), including the Getis-Ord statistic (Getis & Ord, 1992; Ord & Getis, 1995). The application of this statistic to remote sensing data was first shown by Getis (1994). Wulder and Boots (1998) confirmed its utility for this purpose and since then it has been used in various studies to measure the uniformity of surfaces, from identifying coral reef stress (LeDrew et al., 2004) to assessing the quality of vicarious calibration sites (Bannari et al., 2005).

In this study, Bannari et al. (2005) examined the spatial uniformity of the Lunar Lake Playa, Nevada, using both Getis-Ord statistics and the coefficient of variation. They

found that the Getis-Ord statistic was more sensitive to changes in spatial uniformity, and suggested that it should be used for looking at spatial uniformity, while the coefficient of variation was more suited to looking at temporal uniformity.

The formula for the Getis-Ord statistic, G_i^* , is shown below (Ord & Getis, 1995):

$$G_i^*(d) = \frac{\sum_j w_{ij}(d)x_j - W_i^* \bar{x}}{s \left[\frac{W_i^*(n - W_i^*)}{(n - 1)} \right]^{1/2}}$$

Each element of the binary matrix of spatial weights $w_{ij}(d)$ has a weight equal to unity for all the pixels found within distance d of pixel i , and a weight equal to zero for all the pixels found further away than d .

$\sum_j w_{ij}(d)x_j$ is the sum of the Digital Numbers within distance d of pixel i (i included). W_i^* is the number of pixels within the distance d (i included), n is the total number of pixels, x is the DN at row i , column j , \bar{x} is the global mean of x and s is the variance of x (Ord & Getis, 1995). It can be seen that the calculation involves moving this binary matrix across the image, thereby calculating a G_i^* value for the neighbourhood around each pixel.

Two versions of the Getis-Ord statistic exist: G_i does not include the pixel at the centre of the moving window, whereas G_i^* does. It is generally agreed that G_i^* is more appropriate for use in remote sensing (Wulder & Boots, 1998).

An important decision when using Getis-Ord statistics is what value to use for d , which defines the size of the moving window. Bannari et al. (2005) used a 5x5 pixel window ($d = 2$), and Wulder and Boots (1998) used a range of windows from 3x3 to 9x9 pixels. LeDrew et al. (2004) used multiple window sizes, recorded the window size for which the maximum Getis-Ord value was found (the 'Maximum Getis Distance') and used this to classify coral reef stress. When choosing a window size it is important to ensure that a minimum of 8 pixels are used, as this ensures that the resulting Getis-Ord values are normally distributed (Griffith et al., 1996).

4 Method

4.1 Study Images

A selection of images were used for developing and testing the methodology (locations shown in Figure 2). Two IKONOS scenes (Chandlers Ford and Thorne Moor) were used during the development process, and then the method was tested on two more IKONOS scenes (Risley and Kirkbride) and a SPOT scene (Chilbolton; from the NCAVEO field experiment: Milton & NCAVEO Partnership, 2008) to test the applicability of the method to images of differing resolutions. The final part of the methodology was to perform an empirical line method calibration using the automatically selected calibration sites, and examine the results. The SPOT scene was the only image which had corresponding ground data (which would allow this calibration to be carried out) but had a different pixel size to the images the method was developed on, which may affect the results. Therefore a simulated IKONOS image was created from atmospherically corrected Eagle data of Chilbolton (Milton & NCAVEO Partnership, 2008) using the HS2MS routine included with ATCOR-4 (Richter, 2010) to simulate top-of-atmosphere reflectances for the IKONOS sensor.



Figure 2 - Locations of the images used in this study

The site selection process requires a digital surface model of the area covered in the satellite image. These were provided by the NeXTMAP project (NEODC, 2009) which produced Interferometric Synthetic Aperture Radar derived Digital Surface Models (DSMs) and Digital Terrain Models (DTMs) of the whole of the UK at a 5m horizontal resolution and a nominal vertical resolution of 30cm (Intermap, 2004). A DSM was used as this includes the elevations of buildings and other such features which could be used for calibration sites.

When the images were combined with the digital surface models, they were resampled to ensure they were both at the same resolution. The final resolution was always chosen as the lower resolution of the two input files, to avoid interpolating new data. The final pixel sizes were 5m for the IKONOS images and 10m for the SPOT image. Some of the images had areas of cloud in them or areas where the sensor had been saturated, and these were manually masked out before using them.

4.2 Method Overview

The method for automatically selecting calibration sites is split into two stages: firstly the image is processed and thresholds are calculated; and then the image is segmented and classified. The first part is performed in ENVI/IDL (ITTVIS, 2009), and the second in eCognition (Definiens Imaging, 2004b). This partition between the pieces of software allows the first stage to be easily automated using the programmable environment provided with ENVI/IDL; such automation is not possible with eCognition.

Once the calibration sites have been selected, their quality will be assessed using three methods:

1. Comparison of the calibration sites with the list of desirable criteria for calibration sites (Table 2, p20).
2. Assessment by an independent expert
3. Performing an empirical line method calibration using the selected calibration sites and recording the resultant accuracies.

All IDL code written to perform these processes is shown in Appendix D.

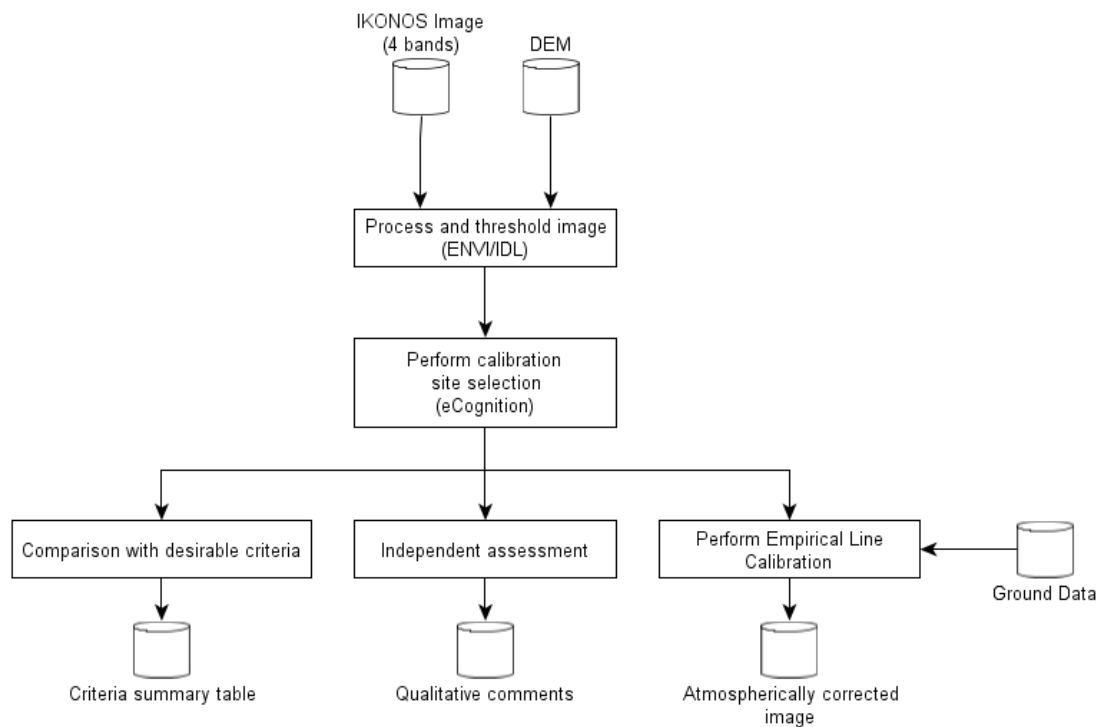


Figure 3 - Overview of the method showing input and output data

4.3 Statistical calculation and thresholding

4.3.1 Assessing spatial uniformity: Getis statistics

Although a function to calculate the Getis statistic across an image is available in ENVI, it appears to calculate G_i rather than G_i^* , and uses a fixed window size of 3 x 3 pixels. The window size was thought to be an important parameter which needed investigation, so a routine to calculate the Getis statistic with a configurable window size was written. It was noted that all previous uses of Getis statistics in remote sensing have used a queen's case pixel neighbourhood, so this was hard-coded into the routine.

An example of the output of the Getis routine for one band of a small image subset is shown in Figure 4.

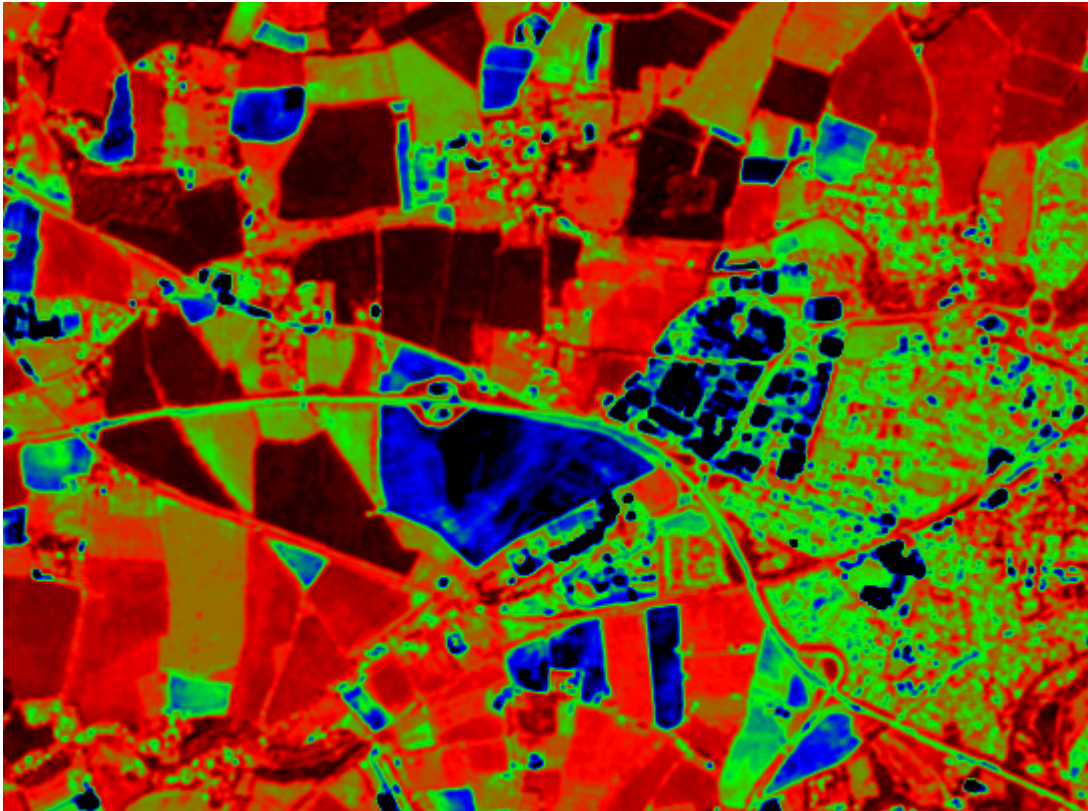


Figure 4 - Example Getis image (subset of Chilbolton image). Black pixels represent uniform areas (either dark or bright).

When checking the output from the Getis calculation routine a peculiarity in the Getis values was noticed. It appears that an area which is very bright and relatively uniform can actually produce a higher Getis value than an area which is less bright, but more uniform. That is, the brightness of an area appears to be affecting the magnitude of the value, whereas Ord and Getis (1995) state that it purely decides the sign. This is investigated more in Appendix B but suggests that image segments should not be ordered by Getis statistic to find the most uniform area, as that technique may return the brightest area instead. This is the reason that thresholding the results from the Getis statistic was investigated.

The Getis statistic routine was written to accept a mask band as an input, allowing areas of the image (such as clouds) to be excluded from the calculation. The moving window was set to be 3x3 pixels ($d = 2$) as this most closely matches the minimum size of calibration site allowed by the eCognition classification (4x4 pixels).

4.3.2 Assessing spectral purity: Endmember extraction

The Pixel Purity Index was investigated for analysing the spectral purity of pixels in the image, but it was found to be very slow as it needed to run for large numbers of iterations to get any useful result. The SMACC routine was far quicker to run, and automatically performed unmixing, producing abundance images.

The SMACC routine takes a parameter giving the number of endmembers to find. Small (2004; 2005) shows that a global sample of Landsat ETM+ scenes can be accurately represented as combinations of three endmembers (High Albedo, Dark and Vegetation), and Rashed et al. (2003) shows that urban scenes (which are important as large proportions of remotely sensed imagery of the UK will include some urban areas) tend to consist of around four endmembers (Vegetation, Impervious surfaces, Soil and Water/Shade). Also, the number of true endmembers which can be found for an image is equal to the number of bands (four for an IKONOS image). Therefore it was decided to configure the routine to find four endmembers. The routine also requires the selection of a constraint to apply to the selected endmembers with the options of: positivity only; sum to less than unity and positivity; and sum to unity. An ENVI tutorial (ITTVIS, 2008) suggests that the sum to unity constraint allows the selection of a dark endmember (which is essential for the selection of good dark calibration sites), but that it should not be used on uncalibrated data. However Wu (2004) suggests that a lack of atmospheric correction has little or no effect on linear spectral unmixing, and preliminary tests appeared to confirm that use of the sum to unity constraint on uncalibrated data produced did not cause problems.

4.3.3 Thresholding

It was decided to apply thresholds to the Getis images and endmember abundances images in ENVI/IDL to avoid having to alter the eCognition class membership functions (described later) when adapting the process for different images.

Originally thresholds were applied to the Getis images and the endmember abundance images using the ENVI *Band threshold to ROI* (Region of Interest) function. However, this only allows absolute thresholds, so a function was written to take a top or bottom

percentile of an image and convert it to a ROI. This allows extraction of the highest and lowest Getis values for the image, which correspond to bright uniform areas and dark uniform areas respectively. When applied to the endmember abundance images it selects the purest pixels in the image, giving a result very similar to that obtained by the PPI, but in a far shorter time.

The thresholds were applied to the images and the results exported as binary masks with values of 1 corresponding to a pixel that was above the threshold, and 0 for all other pixels. Three of these were created: for high Getis values, low Getis values and high endmember abundance values. An iterative process was used to find the most appropriate percentile to use, and it was found that taking the top or bottom 0.3% produced an appropriate number of uniform and pure pixels to go into the classification process.

The advantage of using percentage thresholds is that this allows the routine to automatically adjust itself to each individual image. Using this method, the 0.3% most uniform pixels are selected regardless of the image, whereas absolute thresholds would require adaptation to work with each different image.

4.3.4 Assessing flatness: Topographic Modelling

The Topographic Modelling functions included in ENVI were used to create slope and aspect images from the Digital Surface Model to allow assessment of the flatness of calibration sites.

4.3.5 Automation and User Interface

IDL routines were written to automate the processing and thresholding steps described above and to layerstack the resulting images into one 10-band image. An overview of the process is shown in Figure 5.

A user interface was provided to allow the user to set the percentages used for the thresholding as well as the size of the moving window used by the Getis calculation routine. This was designed to allow the user to have control over how many calibration sites were returned. For example, if the image had very few uniform areas in it then

the user can increase the percentages used for the thresholds to allow more areas to be selected. This possibility is provided in case it needs to be used, but it is expected that the use of percentile thresholds (see above) will allow it to work on any image without adjustment.

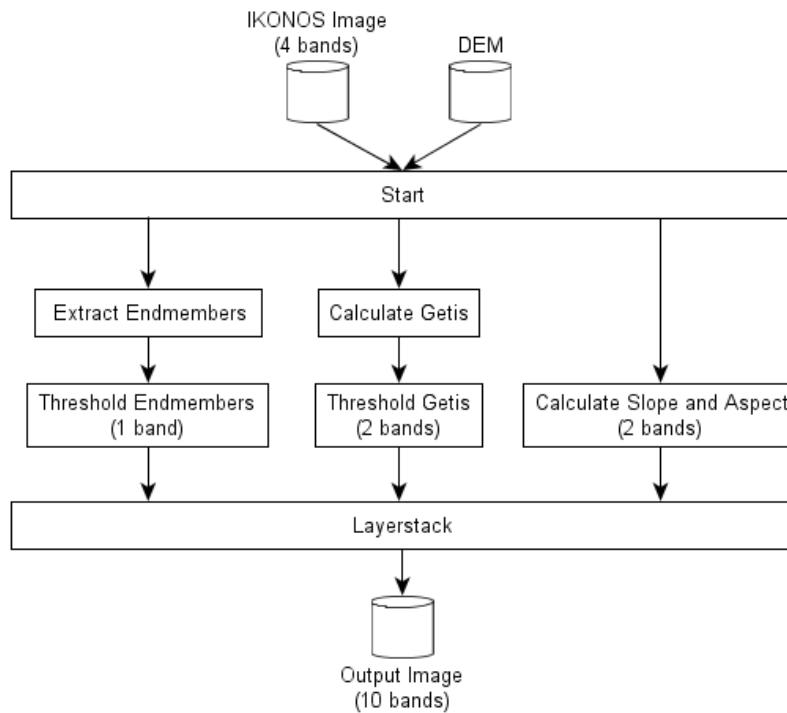


Figure 5 - Overview of the processing and thresholding steps carried out in ENVI/IDL

4.4 Segmentation and classification

4.4.1 Segmentation

The image was segmented using eCognition with the parameters shown in Table 3. Two levels of segmentation were performed: Level 1 using a scale parameter of 10 to produce the segments used in the classification, and Level 2 segmentation using a scale parameter of 0.1 to create a segmentation where each segment contained just one pixel of the image (see Figure 6). The Level 2 classification was then used in the fuzzy classification to assess the proportion of the pixels in each Level 1 segment which had been thresholded by the endmember and Getis thresholding routines.

of each of the larger segments which contained pixels that had been thresholded in the previous process.

The choice of eCognition segmentation parameters has been described as a “black art” (David Holland, Ordnance Survey, personal communication, 2008), particularly with regard to selection of the scale parameter (Hay et al., 2003), and there have been few studies regarding the best parameterisation. Darwish et al. (2003) found that higher scale parameters (that is, larger segments) produced better classification results and that parameterising the segmentation to focus on the spectral values of image objects rather than their shapes appeared to produce the best results. This is one reason why a multi-level segmentation approach was used in this project, as it allows the benefits of the higher scale parameter while also allowing more complex customised features to be defined (see below).

Table 3 - Parameters used for segmentation in eCognition

Parameter	Value
Scale Factor	See text
Shape Factor	0.3
Compactness	0.5
Smoothness	0.5
Included bands	IKONOS Band 1 IKONOS Band 2 IKONOS Band 3 IKONOS Band 4 DEM



Figure 6 - Subset of the Chandlers Ford image showing segmentation at Level 2 (top) and Level 1 (bottom)

4.4.2 Fuzzy classification

eCognition provides various statistics, known as features, which can be calculated for each image object, and it also provides the facility to add customised features to this list. Various customised features were created to be used in rules in the fuzzy classification, and they are described in Table 4.

Table 4 - List of customised features implemented in eCognition, including explanations and calculations used to create them

Feature Name	Description	Calculation
CV (Aspect)	Coefficient of variation of the aspect image	$\frac{\text{Standard Deviation (Aspect)}}{\text{Mean (Aspect)}}$
CV (Slope) (Unused)	Coefficient of variation of the slope image	$\frac{\text{Standard Deviation (Slope)}}{\text{Mean (Slope)}}$
Sum of Dark Getis	Sum of the pixel values in the Level 1 segmentation of the Dark Getis image. As the values in the Dark Getis image are either 1 or 0, this gives the count of the number of pixels which were higher than the threshold.	$\sum \text{Level 2 Dark Getis values}$
Sum of Bright Getis	Sum of the pixel values in the Level 1 segmentation of the Bright Getis image. As above.	$\sum \text{Level 2 Bright Getis values}$
Sum of Endmember Likeness	Sum of the pixel values in the Level 1 segmentation of the endmember abundance image. As above.	$\sum \text{Level 2 Endmember values}$
Fraction like Dark Getis	The fraction of pixels in the image object which were selected by the Dark Getis thresholding routine.	$\frac{\text{Sum of Dark Getis}}{\text{Number of pixels in object}}$
Fraction like Bright Getis	The fraction of pixels in the image object which were selected by the Bright Getis thresholding routine.	$\frac{\text{Sum of Bright Getis}}{\text{Number of pixels in object}}$
Fraction like endmember	The fraction of pixels in the image object which were selected by the endmember abundances thresholding routine.	$\frac{\text{Sum of Endmember Likeness}}{\text{Number of pixels in object}}$
NDVI (Unused)	The average Normalised Difference Vegetation Index (NDVI) of the image object	$\frac{\text{Mean(NIR)} - \text{Mean(Red)}}{\text{Mean(NIR)} + \text{Mean(Red)}}$

A class hierarchy was developed (see Figure 7), using inheritance to reduce the complexity of specifying the rules for each class. In this way, the rules needed to select

the calibration sites were built up gradually. The rules which were implemented are compared to the desirable characteristics of a calibration site (from Table 2, p20) in Table 5.

Table 5 - Comparison of rules implemented in eCognition and the desirable characteristics of a calibration site.

Desirable Characteristic	Implementation
Large	<i>Good Sized</i> rule (thresholds from Table 2, p20)
Range of reflectances (preferably including very bright and very dark targets)	Inherent in both the selection of high and low Getis values (<i>Dark Getis</i> and <i>Bright Getis</i> rules) and the use of endmember values (<i>Like Endmember</i> rule) to ensure the extremities of the pixel cloud are found
Stable over time	Originally assessed by including a rule excluding vegetation (any image object with NDVI > 0.05, from Zhou et al., 2009) but it was found that applying this rule would result in no targets with high NIR values being selected. No other method for assessing stability over time was found, as a time-series of data was not available, so this criterion is no longer assessed.
Spatially homogenous	<i>Dark Uniform</i> and <i>Bright Uniform</i> rules
Flat	<i>Relatively Flat</i> rule
Two or more targets	Controlled by the percentile thresholds set during the thresholding process

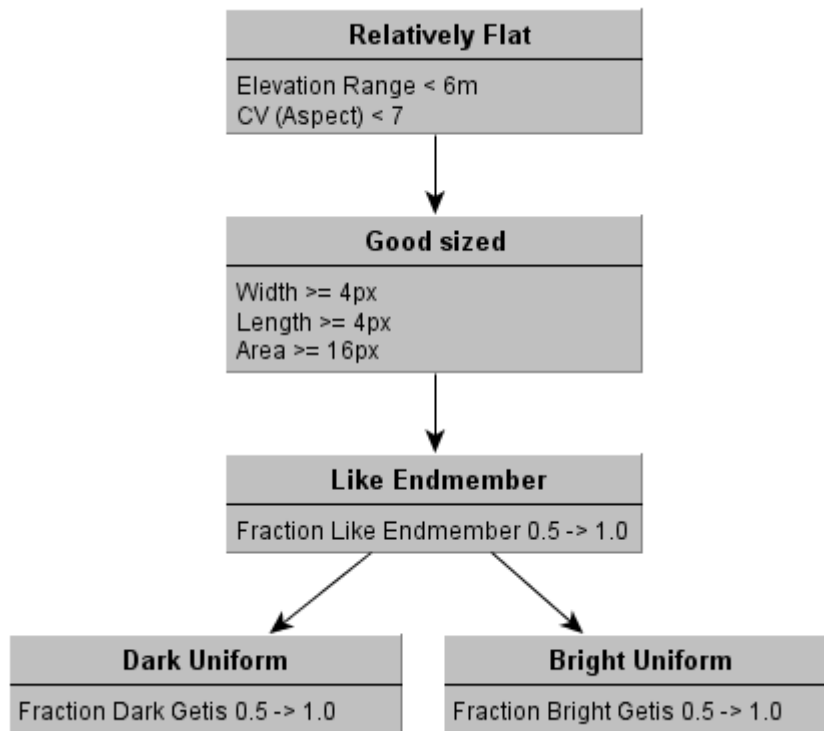


Figure 7 - eCognition class hierarchy. Values specified with X -> Y represent a continuous membership function from X to Y (see text). Classes inherit all rules from the classes above them.

The fuzzy classification options in eCognition were not used for the *Relatively Flat* and *Good Sized* rules as completely fulfilling these rules was thought to be essential. The values for the *Relatively Flat* rule were derived through an iterative process. The threshold for the elevation range was chosen to make sure that buildings with superstructure on them (such as lift machine rooms) were still able to be selected. From examination of the Digital Surface Models used in this project it seems that very few buildings have completely flat roofs (because of issues with drainage) and it was found that setting the threshold for elevation range any lower than 6m excluded nearly all buildings.



Figure 8 - Example of a sawtooth roof on an industrial building in Eastleigh (within the Chandlers Ford IKONOS image). Photographer: Colin Smith, from www.geograph.org.uk

The inclusion of the coefficient of variation of aspect in this rule is to try to exclude sawtooth roofs (see example in Figure 8). These are not desirable for use as calibration targets, as their reflectance varies considerably with changes in insolation angle because of shadows developing between the different sloping components. Various methods for excluding these roofs were examined. Stilla and Jurkiewicz (1999) propose an advanced method which uses histogram analysis of the elevation values of roof. This method can distinguish between many different types of roof, but is unable to be implemented within eCognition as customised features can only be specified using simple algebraic formulae.

It was hypothesized that the variation in slope and aspect would be higher for a sawtooth roof than a flat roof, and this was confirmed by examining slope and aspect images. An iterative process was used to decide an actual value for these thresholds. After further testing, however, the threshold for the slope image was excluded as it was found to exclude water bodies (because it detected the change in slope at the bank of the water body), and checking the coefficient of variation of aspect alone appeared to exclude sawtooth roofs. It was assumed that this technique would not work when the sawtooths themselves were smaller than the resolution of the satellite image. However, testing showed that this technique worked even on the image of Chalcroft Distribution Park shown in the Chandlers Ford image (Figure 9), where each

individual slope component of the sawtooth roof is approximately 3.5m wide (measurements from Google Earth (Google Earth, 2009)) and the satellite image is at a resolution of 5m.

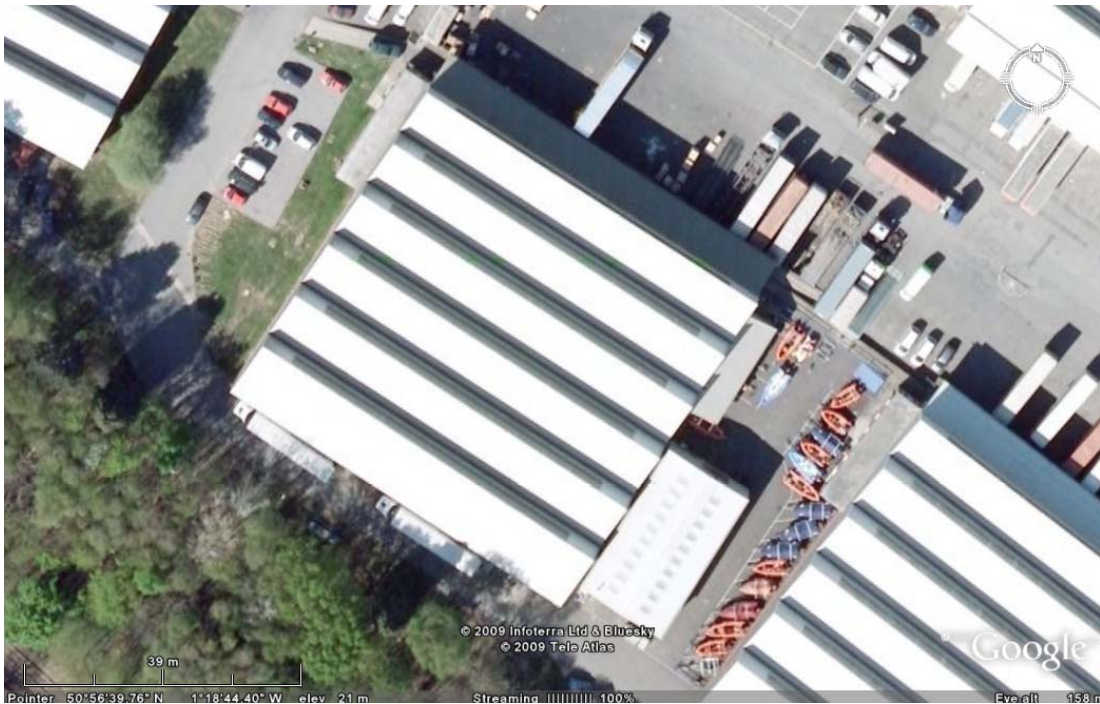


Figure 9 - Aerial photograph of a building in the Chalcroft Distribution Park (Chandlers Ford image). The sawtooth nature of the roof can clearly be seen. (Google Earth, 2009)

Fuzzy membership functions were used for the remaining rules. This involved specifying a range of values which are allowed and letting eCognition assign a membership value for each image object based on the actual value (see Figure 10). A membership value was assigned to the image object for each class that an image object is a member of, and this can be used to see why classes are selected as calibration sites or not. It also allows the final list of calibration sites to be sorted by their membership value, allowing the user to see which image objects fit the criteria most exactly.

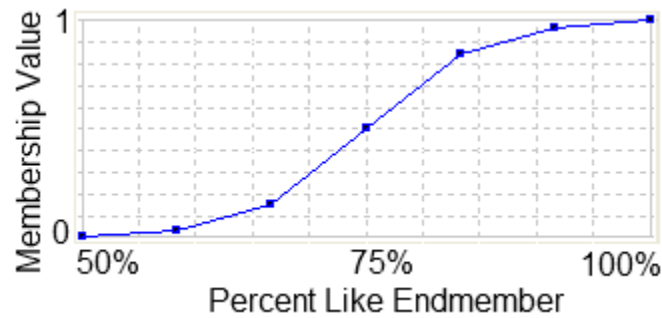


Figure 10 - Membership function graph used for the three fuzzy rules (*Like Endmember*, *Bright Uniform* and *Dark Uniform*). It can be seen that a membership value of 0.5 will be given to an image object which has 75% of its pixels selected as being like endmembers.

As the fuzzy membership functions for *Bright Uniform* and *Dark Uniform* require at least 50% of the pixels in the image object to have been selected as uniform, this will exclude any areas which were masked out of the Getis image, because masked areas were set to zero (representing non-uniform areas) by the Getis statistic calculation routine.

4.4.3 Automation and export

There are limited facilities for automating eCognition in the form of protocols which can be 'recorded' and then run. A protocol was made to perform the required segmentations, load the class hierarchy and then perform the classification, so the user of this routine needs only very slight knowledge of eCognition. Once the classification has been performed the selected calibration sites can be exported to a shapefile which can then be imported into ENVI.

4.5 Comparison with desirable criteria

The best method of assessing the quality of the selected calibration sites is to check whether all of the sites fulfil the desirable criteria for calibration sites listed in Table 2 (p20). Each of these criteria are considered below, the method of checking whether they apply to the selected calibration sites is outlined and the results are shown in a summary table in the results section.

4.5.1 Sites must be large

This was checked by examining the size of each selected site and ensuring it was greater than 4 x 4 pixels.

4.5.2 Sites must have a range of reflectances

This range of reflectances should include very bright and very dark sites to ensure that both ends of the empirical line method regression line are accurately placed. Figure 11 shows histograms of the pixels selected as calibration sites and all pixels in band 3 of the Chilbolton image. It can be seen that the calibration site pixels are generally either very dark or very bright, and in fact consist of some of the brightest and darkest pixels in the scene.

The percentage of calibration site pixels which were in either the top or bottom 10% of the image data was calculated as a quantitative measure of this. As long as there are some calibration site pixels in the top or bottom 10% of the data then the calibration sites are useable, but this statistic provides a useful method of comparing the quality of the sites selected from the different images.

4.5.3 Sites must be stable over time

This was not assessed by the site selection routine, so is not checked in this section.

4.5.4 Sites must be spatially homogenous

Figure 12 shows a subset of the Chilbolton image with bright and dark uniform areas (as selected by the Getis thresholding routine) shown in yellow and green respectively. This appears to show that areas that are expected to be uniform (such as building roofs and lakes) are being selected. However, as the Getis statistic is a relatively new technique, a different technique has been used to validate the results. Coefficient of variation (CV) was calculated across each image using a moving 3x3 pixel window, and the results for each of the calibration sites were examined. Bannari et al. (2005) suggested a CV of 3% as a threshold for uniformity when dealing with ground calibration targets used for sensor calibration. These sites are necessarily more uniform than sites which are likely to be selected for use as atmospheric calibration

sites for routine use and therefore a higher threshold was chosen. It was thought that 9%, a threshold three times Bannari's threshold, was suitable.

4.5.5 Sites must be flat

An important aspect of flatness is the variation of height over an area: the topographic roughness. The surface area ratio (defined as the ratio of 3D surface area to planimetric surface area) can be used as a measure of this (Jenness, 2004). A ratio of 1 shows that an area is completely flat, as the 3D and planimetric surface areas are equal. Completely flat calibration sites will not be expected, but it is difficult to decide where to place the threshold of acceptability. A value of 1.03, that is a 3D surface area 3% greater than the planimetric area, was chosen as the threshold, as this seemed like a suitable value. This also links with Bannari et al.'s (2005) coefficient of variation threshold (see above).

4.5.6 There must be two or more targets

The number of bright and dark targets selected for each image were counted, and at least one site of each type was required for the sites to be acceptable.

4.5.7 Sites must be spread through the image

The spread of sites throughout each image was assessed by eye and recorded in categories of good, moderate and poor.

4.6 Independent assessment

Images showing the selected calibration sites were given to an independent expert (Dr Angela Harris, University of Southampton) for assessment. She provided comments and a score out of ten for each image.

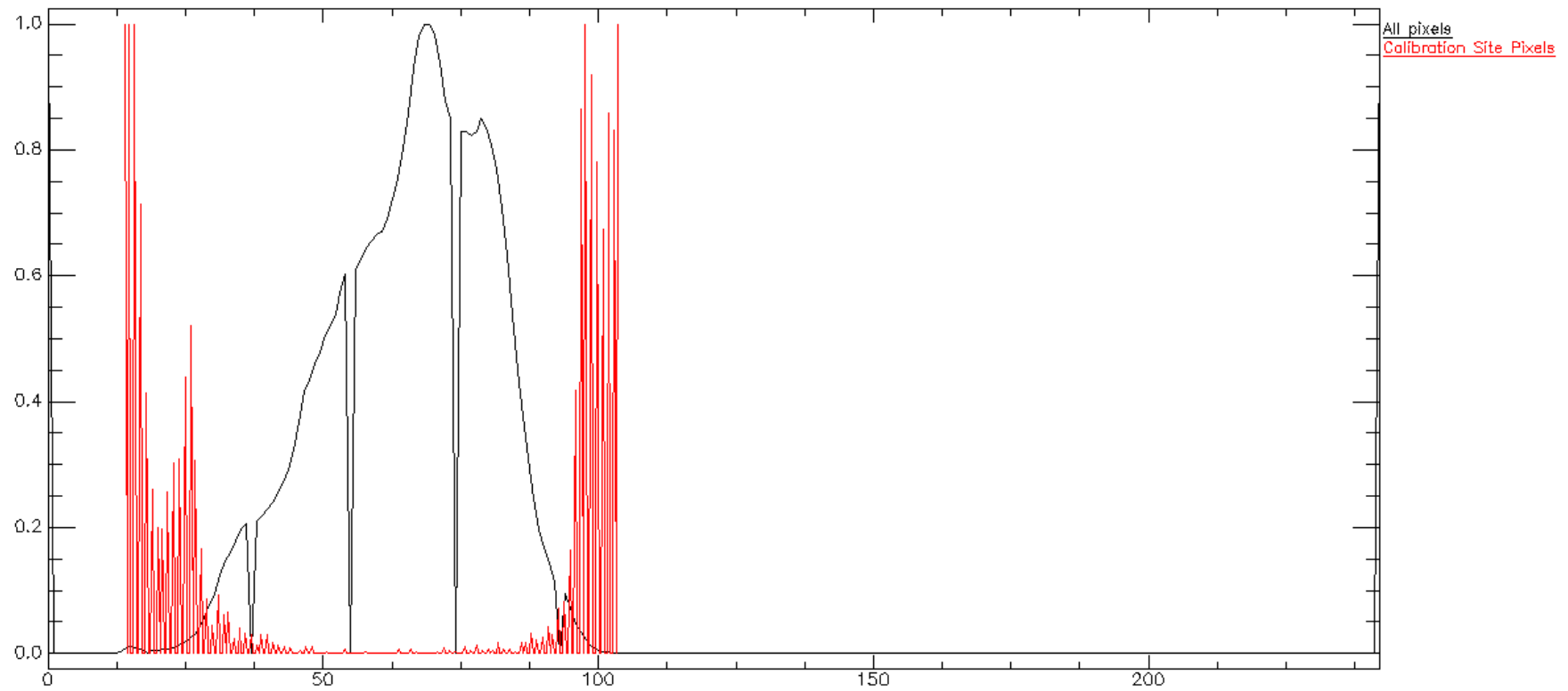


Figure 11 – Histogram of the pixels selected as calibration sites in band 3 of the Chilbolton image (red line) and histogram of all of the pixels in the image (black line) showing that the pixels selected as calibration sites are some of the brightest and darkest pixels in the scene.



Figure 12 - A subset of the Chilbolton image showing dark uniform areas in green and bright uniform areas in yellow, according to the Getis statistic thresholding

4.7 Calibration Test

A routine was written to import each individual polygon in a shapefile to a separate ROI in ENVI. This allowed the calibration site locations to be imported to ROIs, from which mean spectra can be extracted. Field data could then be collected and the Empirical Line Method performed using the built-in ENVI function.

The routine was tested with the SPOT image and the simulated IKONOS image. There was no actual ground data available for use in the Empirical Line Method calculation, so CASI airborne data was geometrically corrected using the AZGCORR utility, calibrated to reflectance using ATCOR-4 (Richter, 2010) and then used as surrogate ground data. The geometrically-corrected CASI data was found to be incorrectly co-registered to the SPOT data, so an image-to-image warp with 10 ground control points spread across the image was used to improve the co-registration to within one pixel.

Five pixels from each of three surface types (Vegetation, Impervious Surface and Water) were pseudo-randomly selected from the corrected SPOT image, and their spectra compared with those from the same locations on the CASI image. A percentage error was then calculated for each band of the spectra at each site using the formula below.

$$\text{Percentage Error} = \frac{|\text{Corrected SPOT Value} - \text{CASI Value}|}{\text{Corrected CASI Value}}$$

5 Results

5.1 Simulated IKONOS analysis

As mentioned above, a simulated IKONOS image was created from Eagle data to be used as one of the test images. However, when the site selection routine was run on this image with the default parameters it did not find any suitable sites. This was investigated, and it was found that the Getis routine was not selecting many uniform sites. It was thought that this is because of the resampling used when converting from the Eagle data (at 1m resolution) to create IKONOS data at 5m resolution. It was therefore decided not to use this image, as it did not appear to have the same uniformity properties as a real IKONOS image.

5.2 Calibration Site Locations

The method was applied to all of the study images described earlier with the default parameters (0.3% for all thresholds). The calibration sites found are shown in the figures below. Red areas represent bright targets and yellow areas represent dark targets, except for the SPOT image where bright targets are shown in green.



Figure 13 - Calibration sites selected within the Chandlers Ford image



Figure 14- Calibration sites selected within the Kirkbride image



Figure 15 - Calibration sites selected within the Risley image



Figure 16 - Calibration sites selected within the Thorne Moor image (rotated 90° anticlockwise)

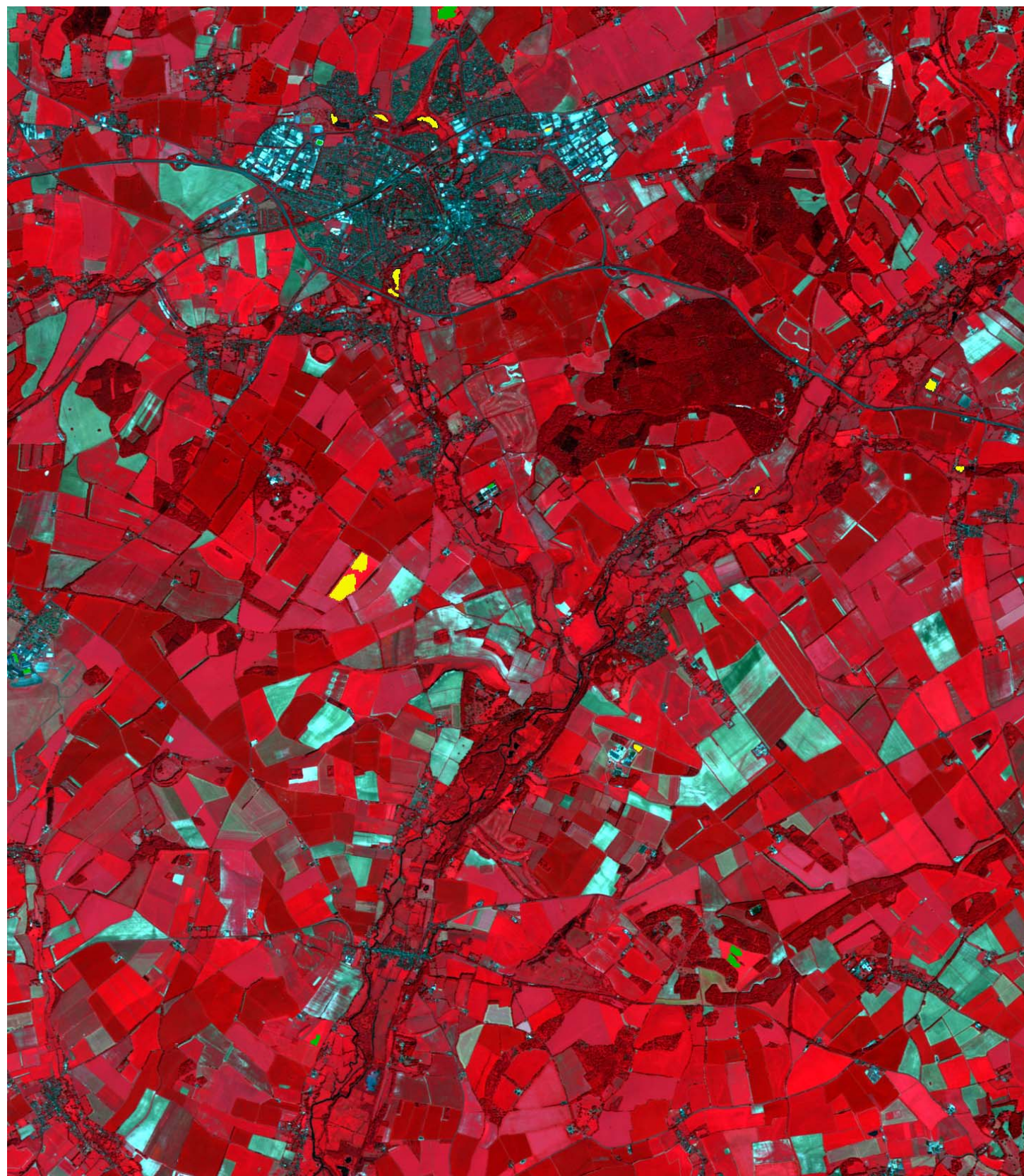


Figure 17 - Calibration sites selected within the Chilbolton image

5.3 Comparison with desirable criteria

Table 7 shows the results of the comparison of the calibration sites selected in each image with the desirable criteria for calibration sites.

5.4 Independent Assessment

Dr Angela Harris' assessments are shown in Table 6.

Table 6 - Qualitative assessment of calibration site selection by Dr Angela Harris

Image	Assessment Comments	Score (out of 10)
Chandlers Ford (IKONOS)	<ul style="list-style-type: none"> Bright buildings appear to be stable – ie. good targets Not sure why some parts of a field have been identified and not others. What is the cutoff? Not sure how well fields will work – should be ok if it's short grass Only one dark target of sufficient size; others appear to be shadows, thus temporal stability is a problem 	7
Kirkbride (IKONOS)	<ul style="list-style-type: none"> Stability of sand in an estuary environment will be low (wetting and drying) over time, but may be ok for a one-off calibration Not many dark sites Edges of building identified instead of centre which "appears" to be more homogenous Medium brightness range appears to be well covered 	6
Risley (IKONOS)	<ul style="list-style-type: none"> Few targets clustered in the same area of the image Dark targets identified well – eg. water 	7
Thorne Moore (IKONOS)	<ul style="list-style-type: none"> Some bright areas in a car-park/industrial unit identified, although some quite small Again includes edges of objects, eg. roofs etc., which could suffer from influences beyond that pixel (eg. neighbouring pixels from the Point Spread Function) Ideally more areas to the north of the image would be useful 	7

Chilbolton (SPOT)	<ul style="list-style-type: none">• Areas of water clearly identified and of sufficient size• Not sure how well the fields will work – depends on vegetation type etc.• Targets well spread throughout the image	8
-------------------	--	---

5.5 Calibration Test

An Empirical Line Method calibration of the SPOT image of Chilbolton was performed using the selected calibration sites. Unfortunately the surrogate ground data did not cover the whole image (see Figure 18), and only five calibration targets were present in both images (see Figure 20 and Table 8).

Table 7 - Comparison of the desirable criteria for calibration sites with the calibration sites selected in each image using the methods specified in section 4.5 (p41).

Image		Large	Range of Bright/Dark	Spatially Homogenous	Flat	Two or more sites	Spread throughout image
Pass	Fail						
Chandlers Ford		All > 4x4 pixels	B1: 38% B2: 39% B3: 39% B4: 90%	B1: 3.6% B2: 4.8% B3: 5.7% B4: 9.4% Avg: 5.8%	Surface Area Ratio: 1.021	Number of Bright: 18 Number of Dark: 9	Moderate
Risley		All > 4x4 pixels	B1: 66% B2: 75% B3: 66% B4: 99%	B1: 3.6% B2: 4.9% B3: 6.8% B4: 10.1% Avg: 6.4%	Surface Area Ratio: 1.016	Number of Bright: 8 Number of Dark: 8	Poor
Kirkbride		All > 4x4 pixels	B1: 60% B2: 60% B3: 60% B4: 39%	B1: 3.1% B2: 4.1% B3: 5.2% B4: 5.1% Avg: 4.4%	Surface Area Ratio: 1.007	Number of Bright: 22 Number of Dark: 0	Moderate
Thorne Moor		All > 4x4 pixels	B1: 21% B2: 67% B3: 62% B4: 94%	B1: 7.4% B2: 10% B3: 13.1% B4: 13.4% Avg: 10.9%	Surface Area Ratio: 1.013	Number of Bright: 23 Number of Dark: 1	Poor
Chilbolton		All > 4x4 pixels	B1: 6% B2: 7% B3: 98%	B1: 6.4% B2: 8.5% B3: 16.3% Avg: 10.4%	Surface Area Ratio: 1.026	Number of Bright: 8 Number of Dark: 11	Good

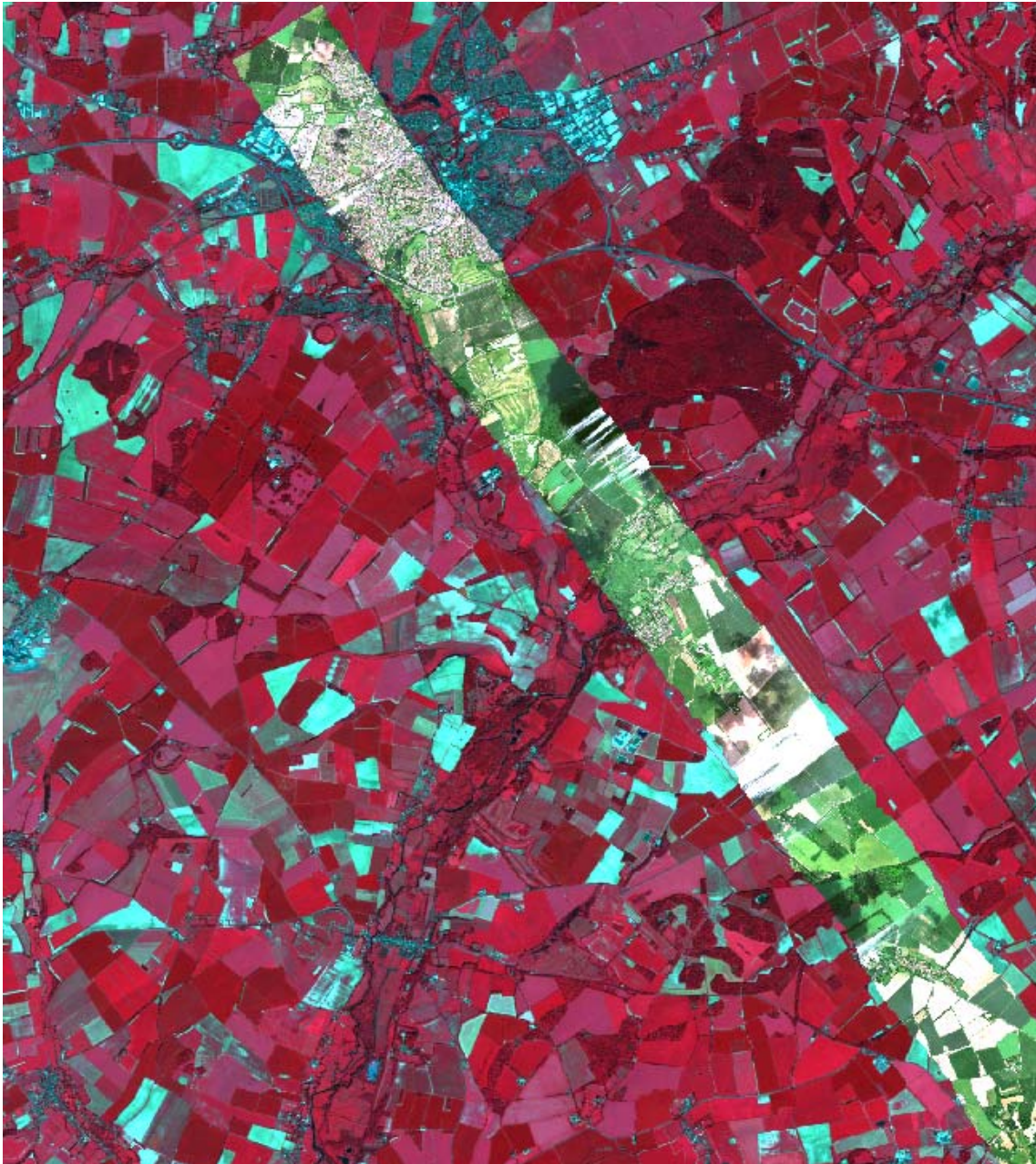


Figure 18 - CASI image overlain on the SPOT image showing the relatively small area where data is available from both images

Table 8 - Information on the calibration targets used in the quantitative assessment

Target Name	Type	Target Description
Building Roof 1	Bright	Bright white roof of a building in an industrial park on the outskirts of Andover
Lake 1	Dark	Small lake in woodland north of Andover
Lake 2 (North)	Dark	Lake just south of Andover
Lake 2 (South)	Dark	Lake just south of Andover
Lake 3	Dark	Lake further south of Andover

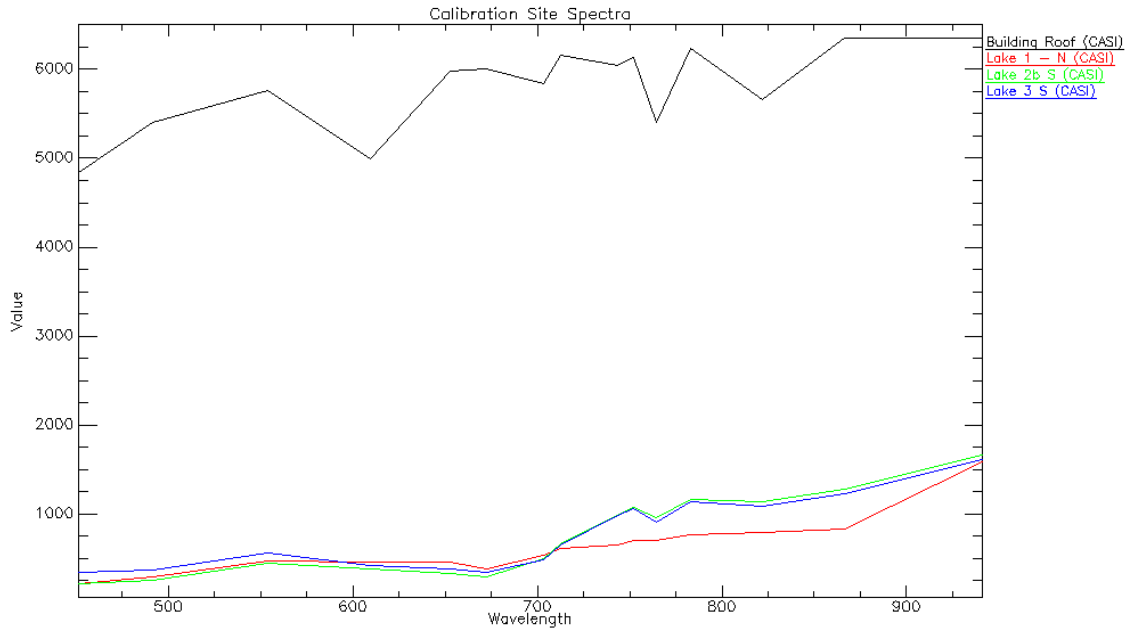


Figure 19 - Average spectra from the calibration sites selected for the calibration, showing the similarity of the three lake spectra.

Table 9 - Average percentage differences between the corrected SPOT and CASI images for a selection of pixels of different surface types

	Vegetation	Impervious	Water	Mean
Green	14.50	35.50	27.39	25.80
Red	20.38	36.85	57.38	38.20
NIR	11.73	49.43	82.16	47.77
Mean	15.54	40.59	55.64	37.26

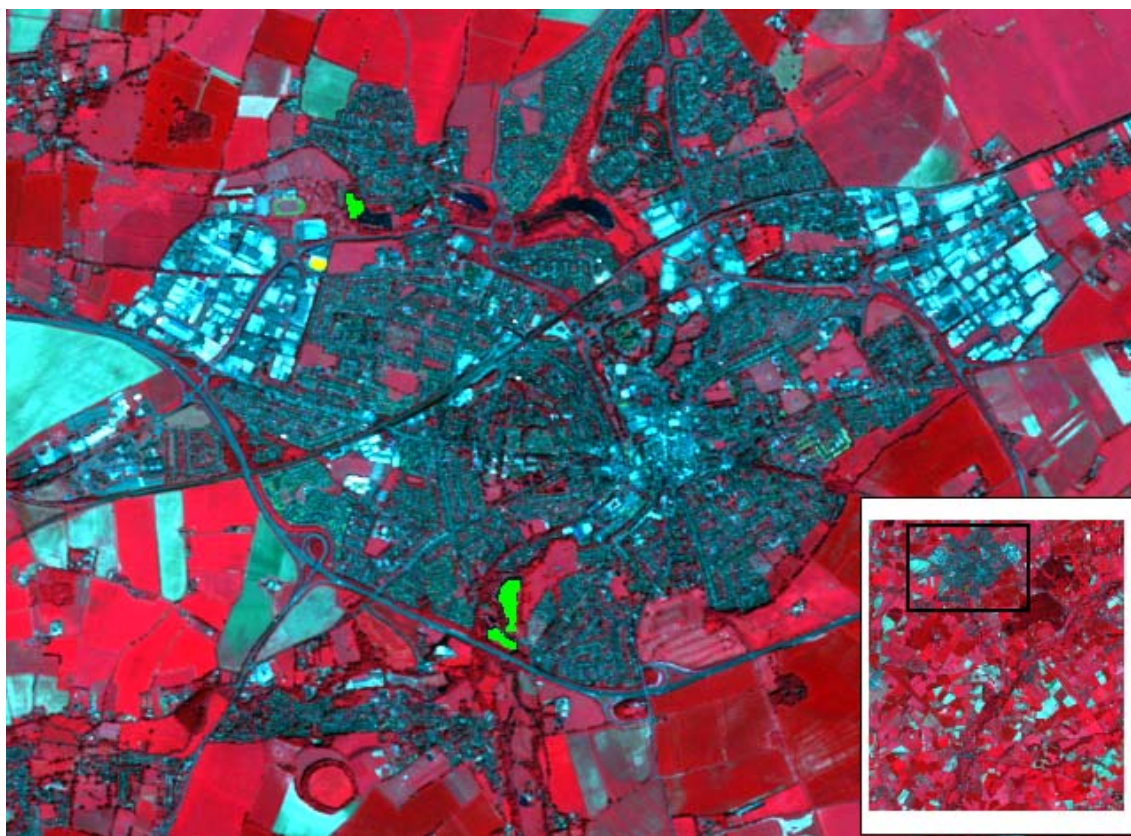


Figure 20 - Subset of SPOT image showing the calibration sites used in the calibration. Inset shows location of image in SPOT scene.

The percentage error of the corrected SPOT image compared with the atmospherically corrected CASI image are shown in Table 9 and Figure 21.

Table 10 - Percentage differences between the corrected SPOT and CASI images for each individual pixel of each surface type

Vegetation			
	Green	Red	NIR
Site 1	0.98	38.08	0.04
Site 2	5.95	19.94	2.17
Site 3	6.62	27.91	14.16
Site 4	22.27	9.51	9.23
Site 5	36.69	6.45	33.06
Impervious Surface			
	Green	Red	NIR
Site 1	5.08	4.50	6.33
Site 2	4.52	8.69	21.87
Site 3	23.37	29.04	90.04
Site 4	38.87	35.84	25.29
Site 5	105.65	106.20	103.61
Water			
	Green	Red	NIR
Site 1	24.47	87.47	102.57
Site 2	33.64	48.38	87.32
Site 3	6.67	29.66	55.80
Site 4	0.68	65.22	77.93
Site 5	71.49	56.19	33.06

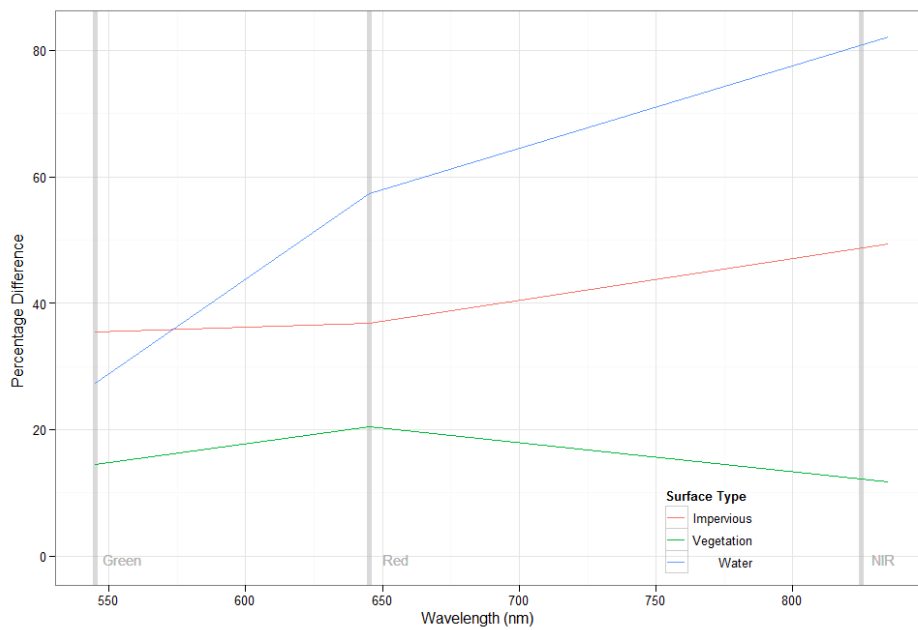


Figure 21 - Graph showing the percentage differences calculated between the corrected SPOT and CASI images, with the three SPOT bands marked

6 Discussion

6.1 Comparison with desirable criteria

Overall, most criteria were met by the selected calibration sites. One image (Chandlers Ford) met all of the criteria, and only one image failed to meet more than one of the criteria. All images pass the criteria of each calibration site being larger than 4x4 pixels.

No dark calibration sites were selected for the Kirkbride image, which would mean that an empirical line method calibration could not be run. All of the problems with other images are more minor, and, although they may affect the quality of the resultant calibration, would not stop a calibration from being carried out.

The thresholds of acceptability for the criteria tests are mostly arbitrary, but the variations in the actual values can give useful insights into the calibration site selection process. For example, the Kirkbride image had the flattest calibration sites, but this is likely to be because of the extensive areas of estuary in the image, all of which are marked on the DEM as having an elevation of 0m. This shows the problems with relying on DEM data which may not reflect the true topography at the moment of satellite image acquisition.

The large range of coefficient of variation values between the images shows the ability of the routine to select the most uniform areas of an image, even when there are major differences between images in terms of the availability of uniform areas.

It is noticeable that there are always fewer dark calibration sites selected than bright calibration sites. The reason for this is likely to be that there are only a few surfaces which are suitable as dark calibration sites. The dark sites which have been selected seem to be water, dense dark vegetation or shadows. It is normally far easier to find sites which are bright in at least one band (such as vegetation which is bright in the NIR band) or bright in most bands (such as a bright white building roof).

The differences between the bands for both spatial uniformity and brightness range show that the NIR normally behaves differently to the visible bands. In most cases the NIR band (Band 4 for the IKONOS images, Band 3 for the SPOT image) has a higher

coefficient of variation. This is likely to be because many of the sites selected for the NIR band will be vegetation, and vegetation is normally less spatially uniform than, for example, a bright building roof.

Also, the NIR band tends to have a higher proportion of the selected pixels in the top or bottom 10% of the image data (up to 98% for the Chilbolton image). This is because the calibration sites for NIR values are normally either water (which has very low NIR values) or vegetation (which has very high NIR values), and very rarely something with values in between.

Achieving a good spread of calibration sites throughout the image is difficult, as land-uses which have large uniform areas (such as lakes or building roofs) are normally only present across part of the image. The Chilbolton image has the best spread of sites, whereas the Risley and Thorne Moor sites perform badly, with sites being concentrated in the east and south respectively. In the Thorne Moor image this is because the northern half of the image is occupied by a large peat bog, which has a very rough surface (both spectrally and topographically).

6.2 Independent Assessment

Overall, the scores given by Dr Harris suggest that the routine picks calibration sites which are fit for purpose. A good number of sites seem to have been selected for most images and many of them are sites which are likely to be relatively temporally stable (such as building roofs (Bretz & Akbari, 1997) or asphalt). However, there are problems, which are detailed below.

One of the most of obvious problems that Dr Harris noticed was the lack of dark calibration sites in the Kirkbride image, and the limited number of dark calibration sites found in some of the other images. It has already been noted that there are a limited number of surface types which are suitable for use as dark calibration sites, but the site selection procedure should be designed to ensure that dark sites are selected even in the most difficult images.

6.2.1 Temporal stability of sites

A distinction should be made here between the calibration sites selected for a one-off calibration, or for use with multiple calibrations. For a one-off calibration where ground data was collected contemporaneously with satellite overpass, the temporal stability of a site is not important. This means that sites such as the estuarine sand sites selected in the Kirkbride image and the vegetation sites selected in all images are likely to be good sites for calibration. However, if the sites are to be used for multiple calibrations then temporal stability is important, and many of these sites would not be suitable. However, it is impossible for the routine to take this into account as a time series of data would be needed to assess the temporal stability of sites.

6.2.2 Spread of sites across the image

Dr Harris commented that the spread of the sites across the image was poor in some images, particularly the Thorne Moor image. However, there is no method in eCognition to ensure that the sites selected are spread across the image so it is impossible to implement a rule to ensure this. It is therefore necessary to check the spread of sites across the image manually after running the site selection method, and, if necessary, change the percentage thresholds to enable more sites to be selected. Some parts of the image naturally have less uniform areas (for example peat bogs) and therefore calibration sites are less likely to be located in these areas.

6.2.3 Adjacency effect problem

Dr Harris commented that the edges of some buildings were selected rather than the centre and that this may cause problems with the influences from neighbouring pixels (because of the Point Spread Function of the sensor; Manslow & Nixon, 2002). It is possible that the edges of the building were selected purely because they happened to be more uniform than the centre of the building. However, there could be a problem with contaminated pixels for these calibration sites. A possible solution to this problem is discussed in section 6.4.2 (p73).

6.2.4 Exclusion of sawtooth roofs

When developing this method it was noted that many bright building roofs are suitable for use as calibration sites, except for sawtooth roofs as these suffer from large changes in spectral reflectance due to changes in insolation angle. A particular effort was made to ensure that sawtooth roofs were not selected, and this was partially successful. Figure 22 shows a subset of the Chandlers Ford image and an aerial photograph of the same area from Google Earth. It can be seen that the only building selected for use as a calibration target is the flat roofed building; all of the sawtooth roofs are excluded.



Figure 22 - Images of Chalcroft Distribution Park from the Chandlers Ford image (left) and Google Earth (right, from Google Earth, 2009) showing the selection only of non-sawtooth roofs

However, the image of a building in the Risley image (Figure 23) shows that some sawtooth roofed buildings are segmented so that each individual piece of roof is an individual image object: this is a problem of oversegmentation (see examples and explanations in Schiewe, 2002). This stops the technique employed to exclude sawtooth roofs from working, as it is looking at aspect variation within each image object, and in this case the aspect is constant for each image object.



Figure 23 - Subset of Risley image showing oversegmentation of a building roof, with each sawtooth segment represented in a separate image object

6.2.5 Overall assessment

The site selection routine seems to select sites which are fit for purpose for the majority of images, and appears to perform best on images that include urban areas and water (such as the Risley, Chandlers Ford and Chilbolton images). This combination of landcover types provides the best conditions for the routine to work as it provides appropriate sites for both bright and dark targets.

6.3 Quantitative Assessment

The average accuracies achieved by the calibration (shown in Table 9, p59) range from 11% to 87% depending on the band and the validation site used. For comparison, accuracies reported in the literature for a variety of atmospheric correction methods including the Empirical Line Method are shown in Table 12. It must be noted that the method used to calculate these percentage error values varies between projects, so the numbers may not be directly comparable.

The best individual accuracy that was achieved in this project (0.04%) appears to be better than those achieved by some of the other projects using the Empirical Line Method, but considerably better than some of the accuracies obtained through the

use of the Refined Empirical Line Method (REL) and the Dark Object Subtraction method (DOS). However, the lowest accuracy is far lower than any other accuracy values reported in the literature. The overall accuracy, averaged over all bands and all validation sites, is just over 37%, which is far worse than any of the results in the literature.

In most of the results from the literature (with the notable exception of Xu & Huang, 2006) there is little difference in accuracies between bands. This is likely to be because calibration sites were chosen which included high and low values for each band. This was not the case in this project, as data availability meant that many of the calibration sites selected by the routine could not be used. Sites low in the NIR band were present (for example, water) but there were no vegetation sites to provide high NIR values. This can be seen in Figure 24, which shows the pixel cloud of the SPOT image, with the different calibration sites used marked on it. If the two main visible axes are taken to represent *Brightness* and *Greenness* (as with the Tasseled Cap transformation, for example Horne, 2003) then it can be seen that the lake site is a good dark site (low brightness and low greenness), and the building roof site is a good site for high brightness, but that there is no site for high greenness. The vegetation label shows where a vegetation calibration site would appear, and using a vegetation calibration site would then cover the three most important endpoints of the data.

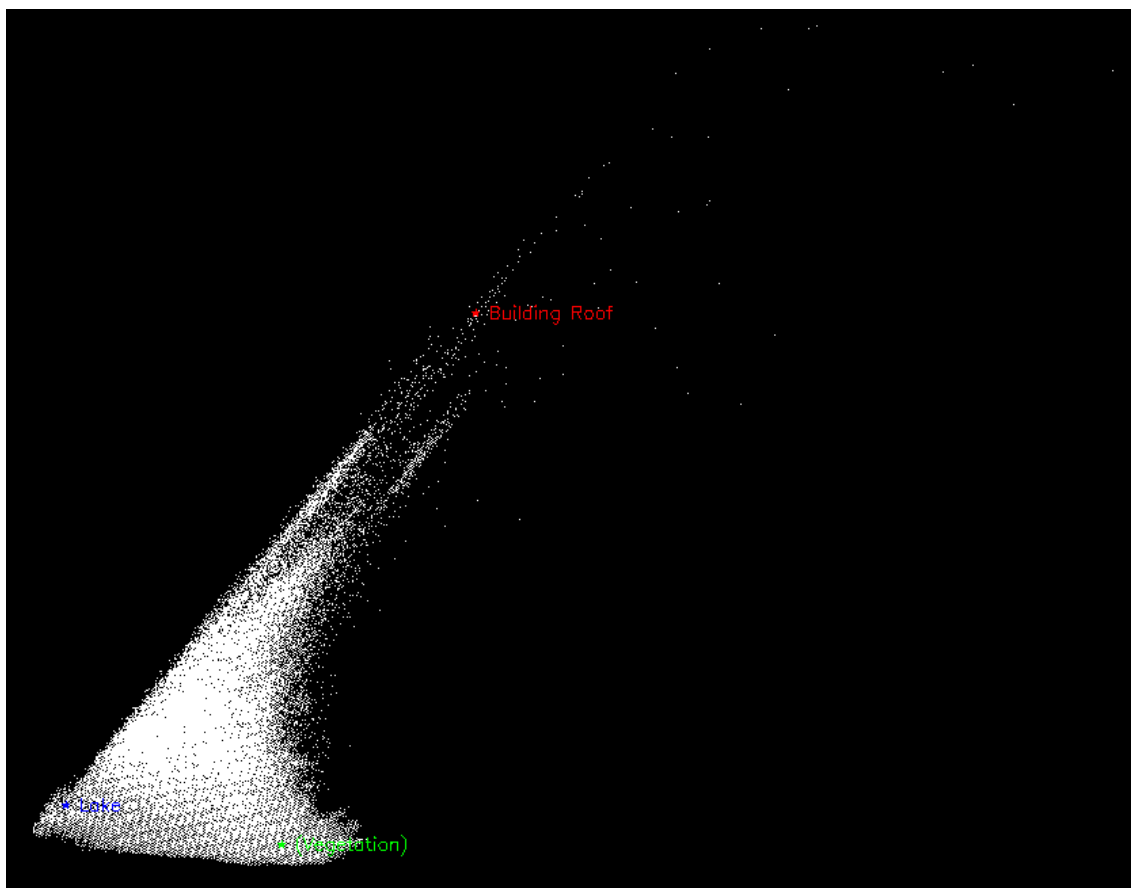


Figure 24 - 3D graph of the pixel cloud from the SPOT data with points marked showing the calibration sites used. The red label is the building roof, the blue label is the average spectra from the lakes and the green label shows where a vegetation calibration site would be placed if one had been available.

The discussion above reflects the low overall quality of the calibration which has been carried out. However it should be noted that this is not necessarily a outcome of the calibration site selection method. The quantitative testing of the method was limited by a number of factors, principally data availability, which are likely to have considerably affected the resulting accuracies. A summary of problems with the calibration which could have affected the resulting accuracies is shown in Table 11.

Table 11 - Problems with the calibration performed in this study, and their causes

Problem	Cause
Sites not spread throughout the SPOT image	Lack of surrogate ground leading to some sites not being able to be used.
Sites do not include a bright and dark site for each band	Lack of surrogate ground data leading to some sites not being able to be used.
Sites possibly including some neighbouring pixels	Imprecise co-registration of SPOT and CASI images.
Comparison not being between exactly the same pixels	Imprecise co-registration of SPOT and CASI images.

Table 12 - Reported accuracies and other details for a number of applications of atmospheric correction approaches in the literature

Method	Sensor	Reported accuracies		Statistical Method	Number of targets	Reference
Empirical Line Method	IKONOS	Blue	1.3%	Mean Absolute Difference	9 targets	Karpouzli and Malthus (2003)
		Green	1.42%			
		Red	1.58%			
		NIR	1.3%			
		Mean	1.4%			
Empirical Line Method	CASI	With 2 targets	1.88%	RMSE	2 or 3 targets	Smith and Milton (1999)
		With 3 targets	0.74%			
Refined Empirical Line Method	IKONOS	Blue	11%	Mean Relative Error	6 bright targets plus RTM-based dark value	Xu and Huang (2006)
		Green	13%			
		Red	3%			
		NIR	5%			
		Mean	8%			
Refined Empirical Line Method	Landsat TM and ETM+	Approximately 1%		Mean Absolute Difference	Various numbers	Moran et al. (2001)
Dark Object Subtraction	Landsat TM	Validation Target 1	4.84%	Not specified	Not applicable	Chavez (1989)
		Validation Target 2	8.42%			
		Mean	6.63%			

6.4 Possible Improvements

Many of the problems with this method are due to the limitations of eCognition. In an ideal world, purpose-built software would be created which would include extra rules which cannot be created in eCognition. These new rules could include the method of Stilla and Jurkiewicz (1999) to identify sawtooth roofs, and measures to ensure a good spread of calibration sites across the image (as this was one of the worst problems identified in the comparison of the selected sites with the desirable criteria).

In a purpose-built piece of software an interactive GUI could be created which would allow the switching on and off of different rules (such as requiring similarity to endmembers, or flatness), in order to see how this changes the calibration sites which are selected. At the moment this can be achieved by running a selection of different eCognition protocols, some of which load class hierarchies that exclude one of the rules (such as the flatness requirement), but this could be much more streamlined. Another option would be to count the number calibration sites selected and automatically adjust the thresholds if very few sites are selected would also be useful.

A limited number of images were available for use in this project. However, in a more complex project a time-series of IKONOS scenes could be provided, thus allowing the temporal stability of the selected calibration sites to be quantified. A processing step could be added using ENVI/IDL to assess how temporally stable the sites are, and then a new eCognition rule could incorporate assessments of temporal stability into the final classification. This would allow assessment of a key criterion for calibration sites: that of temporal stability.

6.4.1 Quantitative Testing Improvements

The quantitative testing performed in this project was of a low quality, mainly because of problems with the availability of ground data. Testing with a comprehensive dataset using all of the calibration sites selected by the routine would enable a far better assessment of how the selection of calibration sites affects the resulting calibration accuracy.

The best way to test the routine would be to choose an image with available ground data, and have calibration sites selected both by the method detailed in this paper and manually by an expert. Two calibrations will then be performed, one with each of the sets of calibration sites, and the resulting accuracies compared.

6.4.2 Pixel Neighbourhood Influence Problem

As mentioned above (Section 6.2.3, p65) there could be a problem with the influence of neighbouring pixels when using the selected calibration site. A sub-project to investigate this is described in Appendix C.

7 Conclusions

The objectives set out at the beginning of this project have all been achieved. A set of criteria has been developed to select calibration sites (Table 2, p20). A method has been devised to select sites based on these criteria (Section 4, p27), and the quality of this method has been assessed by comparison with the original criteria (Section 5.3, p55), by an independent expert (Section 5.4, p55), and by performing an empirical line method calibration (Section 5.5, p56). The overall aim of the project has been fulfilled as an automated system has been created.

The calibration sites selected by this automated system seem to fulfil the majority of the desirable criteria for calibration sites, although it should be remembered that the acceptability thresholds used in this comparison were relatively arbitrary. The independent assessment by Dr Harris suggested that there are some areas in which improvements could be made, but the method selects calibration sites which are fit for purpose. It seems that some images have very few areas which are suitable for use as dark calibration sites, and the site selection routine struggles on these images. Percentile thresholds are used to allow the routine to adapt to different images, and it seems likely that any automatic site selection routine would struggle with these images.

The quantitative assessment provided a large range of accuracies for the different bands and validation sites, making an overall assessment of the accuracy difficult. The average percentage errors of the calibrated SPOT image compared to the surrogate ground data suggests a poor quality calibration. However, data availability problems combined with positional inaccuracy to cause a low quality calibration which was not an accurate reflection of the calibration sites which were used.

Many possible improvements have been suggested above (Section 1.1, p72) and these can be investigated, possibly using a purpose-built piece of software instead of eCognition, as this would allow more complex rules to be defined.

8 Acknowledgements

First of all I would like to acknowledge the huge debt of gratitude I owe to my supervisor, Professor Ted Milton. I am very grateful that I chose him to supervise me for this dissertation, particularly as it has opened a great number of doors to me regarding a future career in academia. His advice has been invaluable, and his patience huge. I hope this dissertation does the work we did together justice.

Olivia, my girlfriend who became my fiancée part way through this project, deserves a special mention here for keeping me sane during the long evenings of working on this project, for helping me to deal with the stress of a large project, and for being a great “rubber duck”¹ on which to test ideas.

My parents have also provided a huge amount of support, as have both sets of grandparents (by inviting me to stay with them on the Isle of Wight, and by being there on the end of a telephone to have a relaxing chat, both of which enabled me to forget about work for a bit).

Gary Watmough provided advice on the usage of eCognition, as well as a good outlet for my rants about some of the ‘quirks’ of this software; Bill Damon provided a friendly face whenever I came into the NCAVEO office to work; and Nick Hamm asked me some hard questions which made me consider the basis of this project more thoroughly.

Finally, I want to acknowledge the University Chaplaincy and the chaplains (both past and present). Without their support (both social and spiritual) I would probably no longer be at University, and this project would never have been completed.

¹ This refers to a method for debugging software which is also applicable to ‘debugging’ scientific arguments. It involves taking the rubber duck from your bath, and very carefully explaining the code line by line to it, which requires you to think very carefully about exactly what each line of code does. During this process one is likely to suddenly realise what the problem is. I found this many times when explaining things to Olivia. For more information see http://en.wikipedia.org/wiki/Rubber_duck_debugging

The opportunity to present this work at the Remote Sensing and Photogrammetry Society Student Conference 2010 was gratefully received, and the preparation for this presentation greatly increased the quality of this report.

Data from the NCAVEO 2006 Field Campaign are provided courtesy of NCAVEO via the NERC Earth Observation Data Centre (NEODC).

9 References

- Adams, J., Smith, M. & Gillespie, A., 1993, 'Imaging spectroscopy: Interpretation based on spectral mixture analysis', *Remote geochemical analysis: Elemental and mineralogical composition*, 7, pp. 145–66.
- Anderson, K. & Milton, E., 2006, 'On the temporal stability of ground calibration targets: implications for the reproducibility of remote sensing methodologies', *International Journal of Remote Sensing*, 27 (16), pp. 3365-74.
- Bannari, A., Omari, K., Teillet, P. & Fedosejevs, G., 2005, 'Potential of Getis statistics to characterize the radiometric uniformity and stability of test sites used for the calibration of Earth observation sensors', *IEEE Transactions on Geoscience and Remote Sensing*, 43 (12), pp. 2918-26.
- Baugh, W. & Groeneveld, D., 2008, 'Empirical proof of the empirical line', *International Journal of Remote Sensing*, 29 (3), pp. 665-72.
- Benz, U. C., Hofmann, P., Willhauck, G., Lingenfelder, I. & Heynen, M., 2004, 'Multi-resolution, object-oriented fuzzy analysis of remote sensing data for GIS-ready information', *ISPRS Journal of Photogrammetry and Remote Sensing*, 58 (3-4), pp. 239-58.
- Berk, A., Anderson, G., Bernstein, L., Acharya, P., Dothe, H., Matthew, M., Adler-Golden, S., Chetwynd Jr, J., Richtsmeier, S. & Pukall, B., 1999, 'MODTRAN 4 radiative transfer modeling for atmospheric correction', in vol. 3756, pp. 348-53.
- Blaschke, T., Lang, S., Lorup, E., Strobl, J. & Zeil, P., 2000, 'Object-oriented image processing in an integrated GIS/remote sensing environment and perspectives for environmental applications', *Environmental information for planning, politics and the public*, 2, pp. 555–70.
- Boardman, J., 1993, 'Automating spectral unmixing of AVIRIS data using convex geometry concepts', in *Summaries of the Fourth JPL Airborne Earth Science Workshop*, Pasadena, CA, USA, pp. 11-4.
- Boardman, J., Kruse, F. & Green, R., 1995, 'Mapping target signatures via partial unmixing of AVIRIS data', in *Summaries of the Fifth JPL Airborne Earth Science Workshop*, Pasadena, CA, USA.
- Bretz, S. E. & Akbari, H., 1997, 'Long-term performance of high-albedo roof coatings', *Energy and Buildings*, 25 (2), pp. 159-67.
- Chavez, P., 1989, 'Radiometric calibration of Landsat Thematic Mapper multispectral images', *Photogrammetric Engineering and Remote Sensing*, 55, pp. 1285-94.

Chavez, P. S., 1996, 'Image-based atmospheric corrections-revisited and improved', *Photogrammetric Engineering and Remote Sensing*, 62 (9), pp. 1025-35.

Cleve, C., Kelly, M., Kearns, F. R. & Moritz, M., 2008, 'Classification of the wildland-urban interface: A comparison of pixel- and object-based classifications using high-resolution aerial photography', *Computers, Environment and Urban Systems*, 32 (4), pp. 317-26.

Cohen, W., Maersperger, T., Yang, Z., Gower, S., Turner, D., Ritts, W., Berterretche, M. & Running, S., 2003, 'Comparisons of land cover and LAI estimates derived from ETM+ and MODIS for four sites in North America: A quality assessment of 2000/2001 provisional MODIS products', *Remote Sensing of Environment*, 88 (3), pp. 233-55.

Darwish, A., Leukert, K. & Reinhardt, W., 2003, 'Image segmentation for the purpose of object-based classification', in *IEEE International Geoscience and Remote Sensing Symposium (IGARSS'03)*, Toulouse, France, vol. 3, pp. 2039-41.

Davranche, A., Lefebvre, G. & Poulin, B., 2009, 'Radiometric Normalization of SPOT-5 Scenes: 6S Atmospheric Model versus Pseudo-invariant Features', *Photogrammetric Engineering and Remote Sensing*, 75 (6), pp. 723-8.

de Jong, S., 1998, 'Imaging spectrometry for monitoring tree damage caused by volcanic activity in the Long Valley caldera, California', *ITC Journal*, 1, pp. 1-10.

Definiens Imaging, 2004a, *eCognition 4 User Guide*, Definiens Imaging, Munich, Germany.

Definiens Imaging, 2004b, *eCognition Professional 4*

Dwyer, J., Kruse, F. & Lefkoff, A., 1995, 'Effects of empirical versus model-based reflectance calibration on automated analysis of imaging spectrometer data: a case study from the Drum mountains, Utah', *Photogrammetric Engineering and Remote Sensing*, 61 (10), pp. 1247-54.

Gallent, N., Howe, J. & Bell, P., 2000, 'New uses for England's old airfields', *Area*, 32 (4), pp. 383-94.

Gao, Y. & Mas, J., 2008, 'A comparison of the Performance of Pixel Based and Object Based Classifications over Images with Various Spatial Resolutions', *Online Journal of Earth Sciences*, 2 (1), pp. 27-35.

Getis, A., 1994, 'Spatial dependence and heterogeneity and proximal databases', *Spatial analysis and GIS*, pp. 105-20.

Getis, A. & Ord, J., 1992, 'The analysis of spatial association by distance statistics', *Geographical Analysis*, 24, pp. 189-206.

Giardino, C. & Brivio, P., 2003, 'The application of a dedicated device to acquire bidirectional reflectance factors over natural surfaces', *International Journal of Remote Sensing*, 24 (14), pp. 2989-96.

Google Earth, 2009, *Image centred on 50° 56' 40.11" N 1° 18' 42.88" W*, <http://earth.google.com> [Accessed 16/12/2009].

Green, A., Berman, M., Switzer, P. & Craig, M., 1988, 'A transformation for ordering multispectral data in terms of image quality with implications for noise removal', *IEEE Transactions on Geoscience and Remote Sensing*, 26 (1), pp. 65-74.

Greiwe, A. & Ehlers, M., 2005, 'Combined analysis of hyperspectral and high resolution image data in an object oriented classification approach', in *Proceedings of 3rd International Symposium on Remote Sensing and Data Fusion over Urban Areas*, Istanbul, Turkey, pp. 13-5.

Griffith, P., Getis, A. & Griffin, E., 1996, 'Regional patterns of affirmative action compliance costs', *The Annals of Regional Science*, 30, pp. 321-40.

Gruninger, J., Ratkowski, A. & Hoke, M., 2004, 'The sequential maximum angle convex cone (SMACC) endmember model', *Proceedings SPIE, Algorithms for Multispectral and Hyper-spectral and Ultraspectral Imagery*, 5425, pp. 1-14.

Hamm, N., Atkinson, P. M. & Milton, E., 2003, 'The combined effect of spatial resolution and measurement uncertainty on the accuracy of empirical atmospheric correction', in *Proceedings of the 2003 IEEE International Geoscience and Remote Sensing Symposium*, Centre de Congres Pierre Baudis, 21-25 July 2003.

Hay, G. J., Blaschke, T., Marceau, D. J. & Bouchard, A., 2003, 'A comparison of three image-object methods for the multiscale analysis of landscape structure', *Photogrammetric Engineering and Remote Sensing*, 57, pp. 327-45.

Horne, J., 2003, 'A tasseled cap transformation for IKONOS images', in *American Society for Photogrammetry and Remote Sensing Conference 2003*, Anchorage, Alaska.

Intermap, 2004, *Intermap Product Handbook and Quick Start Guide*.

ITTVIS, 2008, *ENVI Tutorial: Using SMACC to extract endmembers*, www.itvis.com/portals/0/tutorials/envi/SMACC.pdf [Accessed 15/12/2009].

ITTVIS, 2009, *ENvironment for Visualisation (ENVI) 4.6.1*

Jenness, J. S., 2004, 'Calculating landscape surface area from digital elevation models', *Wildlife Society Bulletin*, 32 (3), pp. 829-39.

Karpouzli, E. & Malthus, T., 2003, 'The empirical line method for the atmospheric correction of IKONOS imagery', *International Journal of Remote Sensing*, 24 (5), pp. 1143-50.

Knight, J., Lunetta, R., Ediriwickrema, J. & Khorram, S., 2006, 'Regional Scale Land Cover Characterization Using MODIS-NDVI 250 m Multi-Temporal Imagery: A Phenology-Based Approach', *GIScience & Remote Sensing*, 43 (1), pp. 1-23.

Kutser, T., Pierson, D. C., Kallio, K. Y., Reinart, A. & Sobek, S., 2005, 'Mapping lake CDOM by satellite remote sensing', *Remote Sensing of Environment*, 94 (4), pp. 535-40.

LeDrew, E. F., Holden, H., Wulder, M. A., Derksen, C. & Newman, C., 2004, 'A spatial statistical operator applied to multirate satellite imagery for identification of coral reef stress', *Remote Sensing of Environment*, 91 (3-4), pp. 271-9.

Lu, D. & Weng, Q., 2006, 'Spectral mixture analysis of ASTER images for examining the relationship between urban thermal features and biophysical descriptors in Indianapolis, Indiana, USA', *Remote Sensing of Environment*, 104 (2), pp. 157-67.

Lu, D. & Weng, Q., 2007, 'A survey of image classification methods and techniques for improving classification performance', *International Journal of Remote Sensing*, 28 (5), pp. 823-70.

Malthus, T. & Karpouzli, E., 2003, 'Integrating field and high spatial resolution satellite based methods for monitoring shallow submersed aquatic habitats in the Sound of Eriskay, Scotland, UK.', *International Journal of Remote Sensing*, 24 (13), pp. 2585-93.

Manslow, J. F. & Nixon, M. S., 2002, 'On the ambiguity induced by a remote sensor's PSF', in G. M. Foody & P. M. Atkinson (eds), *Uncertainty in Remote Sensing and GIS*, Wiley, Chichester, pp. 37-57.

Martínez, P. J., Pèrez, R. M., Plaza, A., Aguilar, P. L., Cantero, M. C. & Plaza, J., 2006, 'Endmember extraction algorithms from hyperspectral images', *Annals of Geophysics*, 49 (1), pp. 93-101.

Matthew, M., Adler-Golden, S., Berk, A., Richtsmeier, S., Levine, R., Bernstein, L., Acharya, P., Anderson, G., Felde, G. & Hoke, M., 2000, 'Status of atmospheric correction using a MODTRAN 4-based algorithm', in *Proceedings of Algorithms for Multispectral, Hyperspectral, and Ultraspectral Imagery VI*, vol. 4049, pp. 199-207.

Meinel, G. & Neubert, M., 2004, 'A comparison of segmentation programs for high resolution remote sensing data', in *ISPRS Congress 2004, Istanbul*, vol. 4, p. 1097.

Milton, E., Lawless, K., Roberts, A. & Franklin, S., 1997, 'The effect of unresolved scene elements on the spectral response of calibration targets: An example', *Canadian journal of remote sensing*, 23 (3), pp. 252-6.

Milton, E. & NCAVEO Partnership, 2008, 'The Network for Calibration and Validation in Earth Observation (NCAVEO) 2006 Field Campaign', in *Proceedings of the Remote Sensing and Photogrammetry Society Conference 2008, 'Measuring change in the Earth system'*, University of Exeter.

Moran, M. S., Bryant, R., Thome, K., Ni, W., Nouvellon, Y., Gonzalez-Dugo, M. P., Qi, J. & Clarke, T. R., 2001, 'A refined empirical line approach for reflectance factor retrieval from Landsat-5 TM and Landsat-7 ETM+', *Remote Sensing of Environment*, 78, pp. 71-82.

NEODC, 2009, *NeXTMap Britain*, <http://www.neodc.rl.ac.uk/?option=displaypage&Itemid=85&op=page&SubMenu=-1> [Accessed 15/01/2010].

Ord, J. & Getis, A., 1995, 'Local spatial autocorrelation statistics: Distributional issues and an application', *Geographical Analysis*, 27, pp. 286-306.

Rashed, T., Weeks, J., Roberts, D., Rogan, J. & Powell, R., 2003, 'Measuring the physical composition of urban morphology using multiple endmember spectral mixture models', *Photogrammetric Engineering and Remote Sensing*, 69 (9), pp. 1011-20.

Richter, R., 2010, *Atmospheric / Topographic Correction for Airborne Imagery: ATCOR-4 User Guide*, DLR - German Aerospace Centre.

Ruiz, C. & Lopez, F., 2002, 'Restoring SPOT images using PSF-derived deconvolution filters', *International Journal of Remote Sensing*, 23 (12), pp. 2379-91.

Schiewe, J., 2002, 'Segmentation of high-resolution remotely sensed data-concepts, applications and problems', *International Archives of Photogrammetry Remote Sensing and Spatial Information Sciences*, 34 (4), pp. 380-5.

Slater, P. N., 1980, *Remote sensing : optics and optical systems*, Addison-Wesley, Reading, Mass.

Small, C., 2004, 'The Landsat ETM+ spectral mixing space', *Remote Sensing of Environment*, 93 (1-2), pp. 1-17.

Small, C., 2005, 'A global analysis of urban reflectance', *International Journal of Remote Sensing*, 26, pp. 661-81.

Smith, G. & Milton, E., 1999, 'The use of the empirical line method to calibrate remotely sensed data to reflectance', *International Journal of Remote Sensing*, 20 (13), pp. 2653-62.

Stilla, U. & Jurkiewicz, K., 1999, 'Reconstruction of building models from maps and laser altimeter data', *Lecture notes in computer science*, pp. 34-46.

Swain, P. H. & Davis, S. M., 1978, *Remote sensing : the quantitative approach*, McGraw-Hill, London.

Teillet, P., Horler, D. & O'Neill, N., 1997, 'Calibration, validation, and quality assurance in remote sensing: A new paradigm', *Canadian journal of remote sensing*, 23 (4), pp. 401-14.

Teillet, P., Thome, K., Fox, N. & Morissette, J., 2001, 'Earth observation sensor calibration using a global instrumented and automated network of test sites (GIANTS)', in vol. 4540, p. 246.

Thomas, N., Hendrix, C. & Congalton, R. G., 2003, 'A comparison of urban mapping methods using high-resolution digital imagery', *Photogrammetric Engineering and Remote Sensing*, 69 (9), pp. 963-72.

USGS, 2009, *The USGS Remote Sensing Technologies Project: Test Site Gallery*, http://calval.cr.usgs.gov/sites_catalog_gallery.php [Accessed 16/12/2009].

Vermote, E., Tanre, D., Deuze, J., Herman, M. & Morcette, J., 1997, 'Second simulation of the satellite signal in the solar spectrum, 6S: An overview', *IEEE Transactions on Geoscience and Remote Sensing*, 35 (3), pp. 675-86.

Wilson, R., 2009, *RTWTools for ENVI*, <http://rtwtools.googlecode.com/> [Accessed 16/12/2009].

Woodside, J., 2009, *A Catalogue of UK Airfields*, <http://www.homepages.mcb.net/bones/06airfields/UK/uk.htm> [Accessed 12/02/2010].

Wu, C., 2004, 'Normalized spectral mixture analysis for monitoring urban composition using ETM+ imagery', *Remote Sensing of Environment*, 93 (4), pp. 480-92.

Wu, J., Wang, D. & Bauer, M., 2005, 'Image-based atmospheric correction of QuickBird imagery of Minnesota cropland', *Remote Sensing of Environment*, 99 (3), pp. 315-25.

Wulder, M. & Boots, B., 1998, 'Local spatial autocorrelation characteristics of remotely sensed imagery assessed with the Getis statistic', *International Journal of Remote Sensing*, 19 (11), pp. 2223 - 31.

Xu, J.-f. & Huang, J.-f., 2006, 'Refined empirical line method to calibrate IKONOS imagery', *Journal of Zhejiang University - Science A*, 7 (4), pp. 641-6.

Yan, G., Mas, J., F, Maathuis, B. H. P., Xiangmin, Z. & Van Dijk, P. M., 2006, 'Comparison of pixelbased and objectoriented image classification approaches a case study in a coal fire area, Wuda, Inner Mongolia, China', *International Journal of Remote Sensing*, 27, pp. 4039-55.

Zhou, W., Huang, G., Troy, A. & Cadenasso, M. L., 2009, 'Object-based land cover classification of shaded areas in high spatial resolution imagery of urban areas: A comparison study', *Remote Sensing of Environment*, 113 (8), pp. 1769-77.

Zhou, W. & Troy, A., 2008, 'An object-oriented approach for analysing and characterizing urban landscape at the parcel level', *International Journal of Remote Sensing*, 29 (11), pp. 3119-35.

- All data will be provided from the NCAVEO Field Experiment – there will be no primary data collection

4. Preliminary work carried out (background references, field visits, etc.)

The following references have been read as background reading:

- Anderson, K. and Milton, E. J., 2006, *On the temporal stability of ground calibration targets: implications for the reproducibility of remote sensing methodologies*
- Bannari, A. et al., 2005, *Potential of Getis Statistics to Characterise the Radiometric Uniformity and Stability of Test Sites Used for the Calibration of Earth Observation Sensors*
- Bhowmick, D., 2009, *Use of an airborne imaging spectrometer as a transfer standard for atmospheric correction of SPOT-HRG data*, MSc thesis, University of Southampton
- Definiens Imaging, 2004, *eCognition User Manual*
- Smith, G. M. and Milton, E. J., 1999, *The use of the empirical line method to calibrate remotely sensed data to reflectance*
- Wolter, M. and Boots, B., 1998, *Local spatial autocorrelation characteristics of remotely sensed imagery assessed with the Getis statistic*

5. Likely problems to be encountered and possible solutions

Problem	Solution
Losing track of goals	Print out copy of this document to review when I feel I'm straying from the goals.
Loss of data due to human error or hardware failure	Perform a backup onto an external hard drive at the end of each day's work. Keep all source code in Subversion version control, hosted at http://code.google.com , and commit changes after all major modifications Perform extra offsite backups after major project milestones reached Backup major project documents to Dropbox
Tasks taking longer than expected	Shift all deadlines forward in time to allow at least an extra month before the final deadline, to allow for slippage.
Losing track of what papers have been read, and misplacing references	Ensure that whenever a paper is read its details are entered into my EndNote library in the 'Dissertation' folder. Perform a final check of all references before submission.
Spelling, punctuation and grammar errors in the final report	Get it proof-read by at least two other people not connected with the project (probably parents).

6. Timeline and key goals (Please include a table for completion or gantt type chart with self-set deadlines to ensure timely completion of the project. Relevant headings might include: 1) literature review; 2) confirmation of methodology; 3) completion of

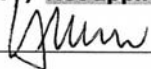
Guidebook – 2009/10

data collection (if appropriate); 4) completion of data analysis; 5) first draft completion; 6) manuscript ready for binding.)

Data acquisition	beginning of June 2009
Data pre-processing	beginning of June 2009
Literature Review	end of June 2009
IDL Getis programming	end of June 2009
Feature selection/extraction	early July 2009
eCognition rule creation	end July 2009
ELM atmospheric correction	end of July 2009
Comparison with RTM and DOS	mid Aug 2009
Comparison with field spectra	mid Aug 2009
Automation of system	end of Aug 2009
First draft	mid Dec 2009
Second draft	early Jan 2010
Third draft	mid Jan 2010
Final draft	end of Jan 2010
Manuscript ready for binding	early Feb 2010

Risk Assessment form **Y / Not applicable**

Ethics Assessment form **Y / Not applicable**

Signature of Supervisor  **Date** 28/4/09

Signature of Student  **Date** 28/04/09

- Programmed routines to automatically create SMACC images and then create percentile-threshold-based classification images from them
- Brought data into eCognition and tried various possibilities of how to classify it
- Wrote code to create a complete image for import into eCognition from the IKONOS file
- Investigated how to create slope and aspect images in ENVI
- Tried lots of methods to try and exclude sawtooth roofs – eventually found one that worked using the CV of slope and the CV of aspect.
- Found and fixed many bugs in my code, all of which were suddenly activated by excluding the DEM image from the processing.
- Investigated RGB image of suitable calibration sites for use as visualisation – both in ENVI and ArcGIS.
- Created false IKONOS image using Eagle data

Writing Up Progress:

- Written first draft of:
 - Introduction
 - Literature Review
- In the process of writing the method – although some parts of this need to wait until all methodological work is finished

Problems Encountered:

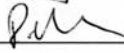
- A number of problematic bugs in my code – all known bugs fixed now though.
- eCognition not working properly, and crashing when performing various functions – workarounds successfully put in place.
- Creating a fake IKONOS image is far more difficult than I thought – and therefore is taking a lot more time than I had allowed in my timetable. This work is ongoing, in consultation with my supervisor.
- Clever methods of building roof type extraction from DEMs are not possible to implement using eCognition – but another simpler method has been found which does work.
- Work from other modules is taking my time away from my dissertation, and causing me to become behind schedule. This is an ongoing problem that I need to deal with by using good time-management skills.

Updated Timetable

Task	Deadline
Practical Work	
Develop method of importing calibration sites to ENVI ROIs	25/11/09
Acquire calibrated data for Chilbolton and resample to SPOT bands	25/11/09
Test ELM on false IKONOS image	25/11/09
Test ELM on SPOT image	25/11/09
Calculate statistics of calibration accuracy for false IKONOS and SPOT images	01/12/09
Finish all practical work on computer – except for exporting pretty images to go in report	01/12/09
Written work	
Complete first draft of Methodology	12/12/09
Complete first draft of Results	06/01/10

Complete first draft of Discussion	06/01/10
Complete first draft of Conclusion	06/01/10
Complete first draft of Appendices (including progress forms, code and any extra maths – for example explanation of the Getis problem)	01/02/10
Complete second draft of entire project	14/02/10
Complete first draft of poster for RSPSoc Student Conference	01/03/10
Complete third draft of entire project	01/03/10
Have project completely finished and ready to hand in	07/03/10
Hand in project	15/03/10

Signature of Supervisor  Date 23/11/09

Signature of Student  Date 23/11/09

11 Appendix B: Getis statistic problem

The calculation of Getis statistics takes into account the brightness of the pixels in the area compared to the rest of the image, and gives large positive results for bright uniform areas and large negative results for dark uniform.

11.1 Problem Statement

The brightness of the area appears to have a larger influence on the Getis statistic than the uniformity of the area. That is, a very bright and relatively uniform area will have a higher Getis value than an area which is not quite as bright, but very uniform.

11.2 Investigation

Various small (10 x 10 pixel) images were created to test the effects of brightness on the value of the Getis statistic. In all cases, the pixel values in the image were chosen using a random number generator (in range 0-255), except for the areas of interest which were manually set to certain values.

The tests were carried out using both the Getis statistic function in ENVI and the Getis statistic code written by the author.

11.2.1 Test 1

Two 3 x 3 pixel test areas were created in the image. The values of each of these areas are shown in Table 13 it can be seen that Area 2 is more uniform than Area 1.

Table 13 - Pixel values for both areas used in Test 1 of the Getis statistic problem

Area 1			Area 2		
255	240	250	240	240	240
249	248	245	240	240	240
252	255	251	240	240	240

However, when the Getis statistics are calculated, Area 1 has a higher Getis statistic than Area 2 (0.0797 and 0.0711 respectively).

11.2.2 Test 2

Another test was carried out to check if the problem occurred only for very large pixel values (as the previous test used values near the limit of 255). Again, two 3 x 3 pixel

test areas were created in the image, in different locations in the image this time. Again, Area 2 is more uniform than Area 1.

Table 14 - Pixel values for both areas used in Test 2 of the Getis statistic problem

Area 1			Area 2		
200	205	203	200	200	200
202	201	208	200	200	200
199	198	200	200	200	200

Again, when the Getis statistics are calculated, Area 1 has a higher Getis statistic than Area 2 (0.0417 compared to 0.0408).

11.2.3 Further Tests

Other tests have been carried out, and they show that this problem is not caused by Area 2 always being perfectly uniform: it occurs even when Area 2 has some slightly different values.

11.3 Impact

It could be argued that the differences between the Getis statistics for these areas are small, but if the Getis statistic is used to rank the most uniform areas in the image then the ranking will be changed by this problem. This was the reason that the threshold-based method for selecting areas was chosen, as areas cannot be reliably ranked using the Getis statistic values.

12 Appendix C: Shrunk calibration site analysis

It was noted in the literature review that Slater (1980) suggested that a ratio of sensor resolution to target size of 1:8 was needed to ensure that four pixels remained uncontaminated in the centre of the target, but in the quantitative testing used in this project the entire calibration site ROI was used, possibly including contaminated pixels. Therefore, a routine has been developed to shrink a ROI by a configurable number of pixels around its edge. This will allow the edge pixels to be excluded from the calibration, possibly leading to increases in the accuracy.

Therefore, a subproject was created to investigate the effect on the calibration accuracy of shrinking the calibration sites in an attempt to remove neighbourhood effects. These effects are introduced through the Point Spread Function (PSF), which represents the contribution of adjacent pixels to the pixel under observation.

Ruiz and Lopez (2002) derived the PSF of the SPOT sensor empirically, and found that it could cause considerable adjacency effects on the image. The central part of their PSF table is reproduced in Table 15, and shows that the contribution of the central pixel to the resulting DN is only 65%, and that up to 4.5% can come from each of the four orthogonally surrounding pixels.

Table 15 - Extract from the central section of the SPOT PSF derived by Ruiz and Lopez (Ruiz & Lopez, 2002). The shaded cell represents the pixel the sensor is observing.

0.0009	0.0016	0.0236	0.0016	0.0009
0.0016	0.0031	0.0448	0.0031	0.0016
0.0236	0.0448	0.6513	0.0448	0.0236
0.0016	0.0031	0.0448	0.0031	0.0016
0.0009	0.0016	0.0236	0.0016	0.0009

From Table 15 it can be seen that the majority of the adjacency effect comes from the pixels which are directly adjacent, therefore it was decided to shrink each of the calibration sites by one pixel around their perimeter, and then run the calibration again. Percentage errors were then calculated using the same validation sites used in the main study.

Table 16 shows the absolute differences between the percentage errors. Negative values indicate an improvement in this version. It can be seen that overall the accuracy decreased by a small amount, but that there were some significant increases for certain bands and validation sites. For example, the percentage error of the NIR band for the water site decreased by almost 20 percentage points. However, it should also be noted that the percentage error for the green band of this site increased by over 10%.

Table 16 - Differences between the percentage error for the normal calibration and the calibration with shrunk calibration sites. Differences are absolute differences in percentage points

	Vegetation	Impervious	Water	Average
Green	-3.52	-0.98	10.22	1.91
Red	6.55	0.87	10.98	6.13
NIR	-0.39	0.04	-19.27	-6.54
Average	0.88	-0.02	0.64	0.50

The results of this sub-project appear to be inconclusive. Shrinking the calibration sites seems to improve the accuracies in certain cases, but makes them significantly worse in other cases. Obviously, adjacency effects should be avoided if possible, but it seems that shrinking the calibration sites to remove these effects is not a good way of increasing the calibration accuracy.

13 Appendix D: IDL Source Code

The code below was written to support this dissertation. Many of the routines created will be useful for other projects, and will be released as part of RTWTools for ENVI (Wilson, 2009) with user-friendly graphical user interfaces added.

CM_REPLICATE, an extension of the IDL REPLICATE routine written by Craig Markwardt is used in the routines below (see <http://cow.physics.wisc.edu/~craigm/idl/arrays.html>).

Getis Statistic Calculation

NewGetis.pro

```

PRO NEWGETIS, event
  ; Use the ENVI dialog box to select a file
  ENVI_SELECT, fid=file,dims=dims,pos=pos, m_fid=m_fid,
m_pos=m_pos, /mask, title="Select the image you want to
perform the Getis calculation on"

  ; If the dialog box was cancelled then stop the procedure
  IF file[0] EQ -1 THEN RETURN

  ; Create dialog box window
  TLB = WIDGET_AUTO_BASE(title="Create Getis Image")

  ; Create dropdown list to select distance value
  list = ['d = 1 (3x3 square)', 'd = 2 (5x5 square)', 'd = 3
(7x7 square)']

  W_Distance = WIDGET_PMENU(TLB, /AUTO_MANAGE, list=list,
uvalue='d')

  ; Create the widget to let the user select file or memory
output
  W_FileOrMem = WIDGET_OUTFM(TLB, /AUTO_MANAGE, uvalue='fm')

  ; Start the automatic management of the window
  result = AUTO_WID_MNG(TLB)

  ; If the OK button was pressed
  IF result.accept EQ 0 THEN RETURN

```

```
    ; Get the details of the file, ready to write to the disk
    if needed
    ENVI_FILE_QUERY, file, fname=fname, data_type=data_type,
xstart=xstart, $
    ystart=ystart, INTERLEAVE=interleave

    ; Get the map info of the file so that we can output it to
    the new file
    map_info = ENVI_GET_MAP_INFO(FID=file)

    ; Initialise the progress bar window - differently
    depending if the output is
    ; to memory or to file
    IF result.fm.in_memory EQ 1 THEN BEGIN
    ENVI_REPORT_INIT, ['Input File: ' + fname, 'Output to
memory'], title='Getis status', base=base, /INTERRUPT
    ENDIF ELSE BEGIN
    ENVI_REPORT_INIT, ['Input File: ' + fname, 'Output File: '
+ result.fm.name], title='Getis status', base=base,
/INTERRUPT
    ENDELSE

    ; Call the function to create the Getis image
    GetisImage = CREATE_GETIS_IMAGE(file, dims, pos, result.d
+ 1, base, m_fid, m_pos)

    IF result.fm.in_memory EQ 1 THEN BEGIN
    ; If the user wanted the result to go to memory then just
    output it there
    ENVI_ENTER_DATA, GetisImage
    ENDIF ELSE BEGIN
    ; If the output is to file then open the file, write the
    binary data
    ; and close the file
    OpenW, unit, result.fm.name, /GET_LUN
    WriteU, unit, GetisImage
    FREE_LUN, unit

    ; Then calculate the values needed to create the header
    file, and create it
    NSamples = dims[2] - dims[1] + 1
    NLines = dims[4] - dims[3] + 1
    NBands = N_ELEMENTS(pos)
```

```

ENVI_SETUP_HEAD, FNAME=result.fm.name, NS=NSamples,
NL=NLines, NB=NBands, $
DATA_TYPE=4, offset=0, INTERLEAVE=interleave, $
XSTART=xstart+dims[1], YSTART=ystart+dims[3], $
DESCRIP="Getis Image Output", MAP_INFO=map_info, /OPEN,
/WRITE
ENDELSE
END

FUNCTION NEWGETIS_NOGUI, file, dims, pos, m_fid, m_pos,
distance
; Get the details of the file, ready to write to the disk
ENVI_FILE_QUERY, file, fname=fname, data_type=data_type,
xstart=xstart, $
ystart=ystart, INTERLEAVE=interleave

; Get the map info of the file so that we can output it to
the new file
map_info = ENVI_GET_MAP_INFO(FID=file)

output_file = fname + "_getis_distance_" +
strcompress(string(distance)) + ".bsq"

; Initialise the progress bar window
ENVI_REPORT_INIT, ['Input File: ' + fname, 'Output File: '
+ output_file], title='Getis status', base=base, /INTERRUPT

; Call the function to create the Getis image - DISTANCE
HARD CODED AS 1
GetisImage = CREATE_GETIS_IMAGE(file, dims, pos, distance,
base, m_fid, m_pos)

help, GetisImage

; If the output is to file then open the file, write the
binary data
; and close the file
OpenW, unit, output_file, /GET_LUN
WriteU, unit, GetisImage
FREE_LUN, unit

; Then calculate the values needed to create the header
file, and create it

```

```

NSamples = dims[2] - dims[1] + 1
NLines = dims[4] - dims[3] + 1
NBands = N_ELEMENTS(pos)
ENVI_SETUP_HEAD, FNAME=output_file, NS=NSamples,
NL=NLines, NB=NBands, $
DATA_TYPE=4, offset=0, INTERLEAVE=interleave, $
XSTART=xstart+dims[1], YSTART=ystart+dims[3], $
DESCRIP="Getis Image Output", MAP_INFO=map_info, /OPEN,
/WRITE

ENVI_OPEN_FILE, output_file, r_fid=fid

return, fid
END

; Creates a Getis image given a FID, the dimensions of the
file, a distance to use for the getis routine
; and a base window to send progress updates to as well as
a fid and pos for the mask (if any)
FUNCTION CREATE_GETIS_IMAGE, file, dims, pos, distance,
report_base, m_fid, m_pos
NumRows = dims[2] - dims[1]
NumCols = dims[4] - dims[3]

NumPos = N_ELEMENTS(pos)

print, NumPos

; Let the progress bar know how many bands we're dealing
with (denom. of fraction)
ENVI_REPORT_INC, report_base, NumPos

FOR CurrPos = 0, NumPos - 1 DO BEGIN
; Send an update to the progress window telling it to let
us know if cancel has been pressed
ENVI_REPORT_STAT, report_base, CurrPos, NumPos

; Get the data for the current band
WholeBand = ENVI_GET_DATA(fid=file, dims=dims,
pos=pos[CurrPos])

; Get the global mean
GlobMean = MEAN(WholeBand)

```

```
; Get the global variance
GlobVariance = VARIANCE(WholeBand)

; Get the number of values in the whole image
GlobNumber = NumRows * NumCols

; Converts a distance to the length of each side of the
square
; Eg. A distance of 1 to a length of 3
DimOfArray = (distance * 2) + 1

NumOfElements = DimOfArray * DimOfArray

; Create the kernel for the summing CONVOL operation
Kernel = FLTARR(DimOfArray, DimOfArray)
Kernel = Kernel + 1

; Create an image where each element is the sum of the
elements within
; d around it
SummedImage = CONVOL(FLOAT(WholeBand), Kernel, /CENTER,
/EDGE_TRUNCATE)

; Create an image where each element is the result of the
top fraction part
; of the getis formula
TopFraction = SummedImage - (FLOAT(NumOfElements) *
GlobMean)

; Calculate the square root bit of the formula and then
create a single variable
; with the bottom fraction part of the formula (this is
constant for all pixels)
SquareRootAnswer = SQRT((FLOAT(NumOfElements) *
(GlobNumber - NumOfElements))/(GlobNumber - 1))
BottomFraction = GlobVariance * SquareRootAnswer

; Create an image with the getis values in it
Getis = FLOAT(TopFraction) / BottomFraction

; If it's the first time then copy the Getis result to
OutputArray,
```

```

; if not then append it to the end of OutputArray
IF (CurrPos EQ 0) THEN OutputArray = Getis ELSE
OutputArray = [ [[OutputArray]], [[Getis]] ]
ENDFOR

; Perform the masking (if needed)
if m_fid NE -1 THEN BEGIN
; Load the mask band
ENVI_FILE_QUERY, m_fid, dims=dims
MaskBand = ENVI_GET_DATA(fid=m_fid, dims=dims, pos=m_pos)

;Apply the mask for each of the bands
FOR i=0, NumPos -1 DO BEGIN
OutputArray[* , *, i] = MaskBand AND OutputArray[* , *, i]
ENDFOR
endif

; Close the progress window
ENVI_REPORT_INIT,base=report_base, /FINISH

; Return the result
RETURN, OutputArray
END

```

ROI Percentile Threshold**roi_percentile_threshold.pro**

```

FUNCTION ROI_PERCENTILE_THRESHOLD, percentage, name, color,
fid=fid, dims=dims, pos=pos,
ensure_above_zero=ensure_above_zero,
ensure_below_zero=ensure_below_zero, bottom=bottom
orig_image_data = ENVI_GET_DATA(fid=fid, dims=dims,
pos=pos)

if KEYWORD_SET(ensure_below_zero) THEN image_data =
orig_image_data[WHERE(orig_image_data LT 0)] ELSE
image_data = orig_image_data
if KEYWORD_SET(ensure_above_zero) THEN image_data =
orig_image_data[WHERE(orig_image_data GT 0)] ELSE
image_data = orig_image_data

if KEYWORD_SET(bottom) THEN sorted_image_indices =
SORT(image_data) ELSE sorted_image_indices =
REVERSE(SORT(image_data))

```

```

len = N_ELEMENTS(image_data)

threshold = image_data[sorted_image_indices[percentage/100
* len]]

print, threshold

if KEYWORD_SET(bottom) THEN BEGIN
  ENVI_DOIT, 'ROI_THRESH_DOIT', dims=dims, fid=fid, pos=pos,
min_thresh=MIN(orig_image_data), $
  max_thresh=threshold, ROI_ID=roi_id, ROI_NAME=name,
ROI_COLOR=color, /NO_QUERY
  ENDF ELSE BEGIN
  ENVI_DOIT, 'ROI_THRESH_DOIT', dims=dims, fid=fid, pos=pos,
$
  min_thresh=threshold, max_thresh=MAX(orig_image_data),
ROI_ID=roi_id, ROI_NAME=name, ROI_COLOR=color, /NO_QUERY
  ENDELSE

return, roi_id
END

```

Automatically create all files needed for eCognition create_files_for_ecog.pro

```

PRO CREATE_FILES_FOR_ECOG, smacc_percentage,
getis_top_percentage, getis_bottom_percentage,
getis_distance, out_file
; Open a dialog box to allow the input IKONOS file to be
selected, along with a mask if needed
  ENVI_SELECT, fid=fid, dims=dims, pos=pos, /mask,
m_fid=m_fid, m_pos=m_pos, title="Select the image,
excluding the DEM band"

; If the dialog was cancelled then just exit
  IF fid EQ -1 THEN RETURN

; Open a dialog box to allow the input DEM band to be
selected
  ENVI_SELECT, fid=dem_fid, dims=dem_dims, pos=dem_pos,
title="Select the DEM band", /band_only

; If the dialog was cancelled then just exit

```

```

IF fid EQ -1 THEN RETURN

; Create the SMACC classification image
smacc_class_fid = CREATE_SMACC_CLASS_IMAGE(fid, dims, pos,
m_fid, m_pos, smacc_percentage)

; Create the Getis classification image
getis_class_fid = CREATE_GETIS_CLASS_IMAGE(fid, dims, pos,
m_fid, m_pos, getis_top_percentage,
getis_bottom_percentage, getis_distance)

; Create the slope and aspect images
slope_aspect_fid = CREATE_SLOPE_ASPECT_IMAGES(dem_fid,
dem_pos)

; Layerstack the above three outputs together, appended on
to the end of the original IKONOS+DEM file
LAYERSTACK_FILES, [fid, smacc_class_fid, getis_class_fid,
slope_aspect_fid], out_file
END

```

Layerstack all the files given in parameters**layerstack_files.pro**

```

; Layerstack every band of the array of fids (input_fids)
together into a specified output file.

```

```

PRO LAYERSTACK_FILES, input_fids, out_name
total_nb = 0

```

```

FOR i=0, N_ELEMENTS(input_fids) - 1 DO BEGIN
ENVI_FILE_QUERY, input_fids[i], nb=nb, ns=ns, nl=nl,
dims=r_dims
pos_to_concat = lindgen(nb)
fids_to_concat = replicate(input_fids[i], nb)

```

```
total_nb = total_nb + nb
```

```
; If it's the first time through then init the arrays
```

```
IF i EQ 0 THEN BEGIN
```

```
output_pos = pos_to_concat
```

```
output_fids = fids_to_concat
```

```
ENDIF ELSE BEGIN
```

```
output_pos = [output_pos, pos_to_concat]
```

```
output_fids = [output_fids, fids_to_concat]
```

```
ENDELSE
```

```
ENDFOR
```

```
; We're assuming that we want the output file to be the
same dims as the last input file - as all the input
; files will be the same size.
output_dims = cmreplicate(r_dims, total_nb)

; Take the projection from the first file
projection = ENVI_GET_PROJECTION(fid=input_fids[0],
pixel_size=pixel_size)

ENVI_DOIT, 'ENVI_LAYER_STACKING_DOIT', fid=output_fids,
pos=output_pos, dims=output_dims, $
out_dt=4, out_name=out_name, out_ps=pixel_size, $
out_proj=projection, r_fid=r_fid
END
```

Create threshold image for high and low Getis values create_getis_class_image.pro

@NewGetis

```
FUNCTION CREATE_GETIS_CLASS_IMAGE, fid, dims, pos, m_fid,
m_pos, top_percentage, bottom_percentage, distance
; If this file is being run manually then the following
must be run first to set up the variables correctly
; ENVI_SELECT, fid=fid,dims=dims,pos=pos, /mask,
m_fid=m_fid, m_pos=m_pos

; Get the filename of the selected file
ENVI_FILE_QUERY, fid, fname=fname

; Create the Getis image, and return the fid of the newly
created image
getis_fid = NEWGETIS_NOGUI(fid, dims, pos, m_fid, m_pos,
distance)

; Initialise the color variable for selecting ROI colors
color = 3

; Get the number of bands of the Getis image
ENVI_FILE_QUERY, getis_fid, nb=nb

; Create the arrays ready to hold the band lists and the
ROI IDs
pos = lindgen(nb)
```

```
top_roi_ids = lonarr(N_ELEMENTS(pos))
bottom_roi_ids = lonarr(N_ELEMENTS(pos))

; For each band in the Getis image
FOR i=0, N_ELEMENTS(pos)-1 DO BEGIN
  print, "Doing band " + string(i)
  ; Get the high Getis values (bright uniform areas)
  top_roi = ROI_PERCENTILE_THRESHOLD(top_percentage, "Band "
+ strcompress(string(pos[i])) + " top", color,
fid=getis_fid, dims=dims, pos=pos[i], /ensure_above_zero)

  ; Set up the new colour for the next ROI and add to the
list of the Top ROIs
  color = color + 1
  top_roi_ids[i] = top_roi

  ; Get the low Getis values (dark uniform areas)
  bottom_roi = ROI_PERCENTILE_THRESHOLD(bottom_percentage,
"Band " + strcompress(string(pos[i])) + " bottom", color,
fid=getis_fid, dims=dims, pos=pos[i], /bottom,
/ensure_below_zero)

  ; Set up the new colour for the next ROI and add to the
list of the Bottom ROIs
  color = color + 1
  bottom_roi_ids = bottom_roi
ENDFOR

; Initialise an array to store the FIDs of the created
classification images
fids = lonarr(2)

; Export the bottom ROIs
ENVI_DOIT, 'ENVI_ROI_TO_IMAGE_DOIT',
class_values=replicate(1, N_ELEMENTS(pos)), FID=getis_fid,
ROI_IDS=bottom_roi_ids,
out_name=fname+"BottomGetisClass.bsq", r_fid=r_fid
fids[0] = r_fid

; Export the top ROIs
ENVI_DOIT, 'ENVI_ROI_TO_IMAGE_DOIT',
class_values=replicate(1, N_ELEMENTS(pos)), FID=getis_fid,
```

```

ROI_IDS=top_roi_ids, out_name=fname+"TopGetisClass.bsq",
r_fid=r_fid
fids[1] = r_fid

; Do the layerstacking of the classification images

poss = lonarr(N_ELEMENTS(fids))
dims = lonarr(5, N_ELEMENTS(fids))

FOR i=0, N_ELEMENTS(fids)-1 DO BEGIN
ENVI_FILE_QUERY, fids[i], nb=nb, dims=r_dims
poss[i] = nb - 1
print, nb - 1
dims[* , i] = r_dims
ENDFOR

projection = ENVI_GET_PROJECTION(fid=fids[0],
pixel_size=pixel_size)

ENVI_DOIT, 'ENVI_LAYER_STACKING_DOIT', fid=fids, pos=poss,
dims=dims, $
out_dt=1, out_name=fname+"_GetisClassStacked.bsq",
out_ps=pixel_size, $
out_proj=projection, r_fid=r_fid

; Return the layerstacked image with both the high and low
Getis classifications in it
return, r_fid

END

```

Create threshold for the high SMACC values

create_smacc_class_image.pro

```

@CREATE_SMACC_ROI_CLASS_IMAGE
FUNCTION CREATE_SMACC_CLASS_IMAGE, fid, dims, pos, m_fid,
m_pos, percentage
; If this file is being run manually then the following
must be run first to set up the variables correctly
; ENVI_SELECT, fid=fid,dims=dims,pos=pos, /mask,
m_fid=m_fid, m_pos=m_pos

; Get the filename of the given file

```

```

ENVI_FILE_QUERY, fid, fname=fname

; Perform the SMACC endmember extraction asking for 4
endmembers, with the constraint of
; summing to unity
ENVI_DOIT, "ENVI_SMACC_DOIT", m_fid=m_fid, m_pos=m_pos,
fid=fid, dims=dims, pos=pos, $
n_endmembers=4, abund_name=fname+"_abund.bsq",
abund_r_fid=abund_fid, method=2, $
out_name=fname+"_speclib.sli", r_fid=r_fid

; Find out how many bands the image has (in case the
number of endmembers above has been changed)
ENVI_FILE_QUERY, abund_fid, dims=r_dims, nb=nb

; Create a list of all the bands in the image so that all
of them can be processed
smacc_pos = lindgen(nb)

; Create the classification image from the SMACC image
r_fid = CREATE_SMACC_ROI_CLASS_IMAGE(percentage,
abund_fid, r_dims, smacc_pos)

; Return the FID of the classification image
return, r_fid
END

```

Perform the threshold processing for the SMACC create_smacc_roi_class_image.pro threshold image creation

```

FUNCTION CREATE_SMACC_ROI_CLASS_IMAGE, percentage, fid,
dims, pos
; If the dialog box was cancelled then stop the procedure
IF fid[0] EQ -1 THEN RETURN, -1

ENVI_FILE_QUERY, fid, fname=fname

; Create an array to hold the roi_ids returned by the
Percentile Threshold function
roi_ids=lonarr(n_elements(pos))

; For each band...
FOR i=0, N_ELEMENTS(pos)-1 DO BEGIN
; Create a name for the ROI

```

```

name = "Band " + STRCOMPRESS(STRING(i)) + " " +
STRCOMPRESS(STRING(percentage, FORMAT="(f5.3)")) + "%"

print, name

;Create the ROI using a percentile threshold
roi_id = ROI_PERCENTILE_THRESHOLD(percentage, name, 2+i,
fid=fid, dims=dims, pos=pos[i], /ensure_above_zero)

; Put the ROI ID into the array
roi_ids[i] = roi_id
ENDFOR

; Convert the ROIs to a classification image where every
pixel that is in any of the ROIs gets given a value of 1
ENVI_DOIT, 'ENVI_ROI_TO_IMAGE_DOIT',
class_values=replicate(long(1), N_ELEMENTS(pos)), FID=fid,
ROI_IDS=roi_ids, out_name=fname+"_SMACC_ClassImage.bsq",
r_fid=r_fid

return, r_fid
END

```

Create slope and aspect images**create_slope_aspect_images.pro**

```

; Takes the fid, pos and dims of a DEM band and creates
slope and aspect images from it
FUNCTION CREATE_SLOPE_ASPECT_IMAGES, dem_fid, dem_pos
; Get the name and dimensions of the DEM band
ENVI_FILE_QUERY, dem_fid, fname=fname, dims=dem_dims

; Get the pixel size of the DEM band
projection = ENVI_GET_PROJECTION(fid=dem_fid,
pixel_size=pixel_size)

; Perform the topographic processing, outputting to a file
ENVI_DOIT, 'TOPO_DOIT', BPTR=[0,1], fid=dem_fid,
pos=dem_pos, $
out_name=fname+"_slope_aspect.bsq", dims=dem_dims,
r_fid=r_fid, $
kernel_size=3, pixel_size=pixel_size

; Return the FID of the file created above
return, r_fid

```

END

Convert Shapefile to individual ROIs

shp_to_roi.pro

```
; The procedure below is specifically written to work with
.shp files exported
; from eCognition for a project by Robin Wilson, and may
not work for other uses
; The idea is that the shape file, and the image file to
associate the ROIs with
; are passed to the procedure, and an individual ROI for
each shape file polygon
; is created. However, there is attribute checking (see
notes in comments), so it
; doesn't do all of the input shapefile.
;
; Adapted from class_image_stats.pro by Andy Pursch,
available at
http://www.ittvis.com/UserCommunity/CodeLibrary.aspx
;
PRO SHP_TO_ROI, shape_file, image_file
  ; Return to the calling program if there is an error
  ON_ERROR, 2

  ; Open (and check) the image file.
  ENVI_OPEN_FILE, image_file, r_fid=fid,
/no_interactive_query, /no_realize
  IF fid EQ -1 THEN BEGIN
void = DIALOG_MESSAGE('Unable to open image file', /error)
RETURN
  ENDIF

  ; Retrieve information about the file
  ENVI_FILE_QUERY, fid, file_type=file_type, nl=num_lines, $
ns=num_samps, num_classes=num_classes

  ; Open (and check) the shape file. Use the IDL shapefile
object since ENVI's
  ; shapefile API is not exposed to the user.
  shape_file_obj = OBJ_NEW('idlffshape', shape_file)
  IF NOT OBJ_VALID(shape_file_obj) THEN BEGIN
void = DIALOG_MESSAGE('Unable to access shape file',
/error)
RETURN
```

```
ENDIF
; Get the number of entities and the entity type.
shape_file_obj->GetProperty, N_ENTITIES=num_ent, $
ENTITY_TYPE=ent_type

; Get the info for all attributes.
shape_file_obj->GetProperty, ATTRIBUTE_INFO=attr_info

; Loop through the entities, converting each to an ROI,
getting/computing the stats,
; writing out the stats.
icnt=0

ENVI_BATCH_STATUS_WINDOW, /ON
repStr='Processing Classification Image'
ENVI_REPORT_INIT, repStr, BASE=repBase, TITLE='Calculating
ROI Statistics'
ENVI_REPORT_INC, repBase, num_ent
WIDGET_CONTROL, /HOURGLASS

; Start looping over all individual cells from the
shapefile
FOR i=0, num_ent-1 DO BEGIN

; Update the processing status bar
ENVI_REPORT_STAT, repBase, i, num_ent-1

; First, get the vertices for the entity.
this_entity = shape_file_obj -> GetEntity(i) ; Could add
the attributes keyword here.
these_vertices = *(this_entity.vertices)
attr = shape_file_obj->getAttributes( i)

; Check the attributes. If the best class field is -1 then
a class was not
; assigned.
IF attr.attribute_2 EQ -1 THEN CONTINUE ; ELSE $
; IF attr.attribute_2 EQ 1 THEN name = "bright" ELSE $
; IF attr.attribute_2 EQ 2 THEN name = "dark"

print, "these_vertices"
print, these_vertices
```

```
x_file_coords = reform(these_vertices[0,*])
y_file_coords = reform(these_vertices[1,*])

;x_file_coords = num_samps - x_file_coords
y_file_coords = num_lines - y_file_coords

; Do shape file polygon entities get returned as a closed
; set of coordinates or if it's just implicit, let's
check. ROIs require
; polygons to be explicitly closed.
last_element_index = N_ELEMENTS(x_file_coords)-1
IF x_file_coords[0] NE x_file_coords[last_element_index]
THEN BEGIN
x_file_coords = [x_file_coords, x_file_coords[0]]
y_file_coords = [y_file_coords, y_file_coords[0]]
ENDIF

print, "HELLO, ROBIN HERE!"
print, x_file_coords

; Since the overlay grid covers a larger geographic extent
than the image some of the
; polygons will lie off the image. We can skip them.
IF TOTAL(x_file_coords LT 0) EQ 0 AND TOTAL(y_file_coords
LT 0) EQ 0 AND $
TOTAL(x_file_coords GT NUM_SAMPS) EQ 0 AND
TOTAL(y_file_coords GT NUM_LINES) EQ 0 THEN BEGIN
; define counter for the the number of valid ROIs
icnt++

; Now that we're in file coordinates, make an roi.
this_roi_id = ENVI_CREATE_ROI(nl=num_lines, ns=num_samps,
name=attr.attribute_1+string(i))
ENVI_DEFINE_ROI, this_roi_id, /polygon,
xpts=x_file_coords, ypts=y_file_coords

print, "-----"
print, x_file_coords

ENDIF
ENDFOR
```

```
ENVI_REPORT_INIT, BASE=repBase, /FINISH

; Destroy shapefile object to free up memory
OBJ_DESTROY, shape_file_obj

PRINT, 'Total number of Valid ROIs found: ', icnt
END
```

Shrink ROIs

shrink_roi.pro

```
; Shrink an individual ROI from the file specified with fid
PRO SHRINK_ROI, fid, roi_id
; Get the number of samples
ENVI_FILE_QUERY, fid, ns=ns, nl=nl

; Get the array of 1D points then convert them to actual x
and y co-ords
points = ENVI_GET_ROI(roi_id)

; If there are no points in the ROI then exit
if points[0] EQ -1 THEN RETURN

; Create the image array
image_array = intarr(ns, nl)

; Extract the point indices to X and Y co-ordinates
point_indices = ARRAY_INDICES(image_array, points)

; Set the area covered by the ROI to 1 in the image_array
image_array[point_indices[0, *], point_indices[1, *]] = 1

; Create the kernel for the summing CONVOL operation - no
diagonals
Kernel = FLTARR(3, 3)
Kernel[0, *] = [0, 1, 0]
Kernel[1, *] = [1, 1, 1]
Kernel[2, *] = [0, 1, 0]

; Create an image where each element is the sum of the
elements within
; d around it
```

```
summed_image = CONVOL(image_array, Kernel, /CENTER,  
/EDGE_TRUNCATE)  
  
; Select the indices where the pixels are entirely  
surrounded by other pixels  
; That is, all the pixels we want to keep in the shrunk  
ROI  
where_answer = WHERE(summed_image EQ 5, count)  
  
IF count EQ 0 THEN RETURN  
  
new_indices = ARRAY_INDICES(summed_image, where_answer)  
  
; Extract the X and Y indices from the array  
new_x_indices = reform(new_indices[0, *])  
new_y_indices = reform(new_indices[1, *])  
  
; Create the new ROI and associated the points with it  
new_roi_id = ENVI_CREATE_ROI(nl=nl, ns=ns, name="Shrunk  
ROI")  
ENVI_DEFINE_ROI, new_roi_id, /point, xpts=new_x_indices,  
ypts=new_y_indices  
END  
  
; Shrink all the ROIs associated with an image  
PRO SHRINK_ALL_ROIS  
; Select the file the ROIs are associated with  
ENVI_SELECT, fid=fid  
  
; Get the list of ROIs and run through it shrinking all of  
them  
roi_ids = ENVI_GET_ROI_IDS(fid=fid)  
FOR i = 0, N_ELEMENTS(roi_ids) - 1 DO BEGIN  
print, "DOING ROI ID ", roi_ids[i]  
SHRINK_ROI, fid, roi_ids[i]  
ENDFOR  
END
```